



**HAL**  
open science

# Optimal description of Blaschke–Santaló diagrams via numerical shape optimization

Ilias Ftouhi

► **To cite this version:**

Ilias Ftouhi. Optimal description of Blaschke–Santaló diagrams via numerical shape optimization. 2022. hal-03646758

**HAL Id: hal-03646758**

**<https://hal.science/hal-03646758v1>**

Preprint submitted on 19 Apr 2022

**HAL** is a multi-disciplinary open access archive for the deposit and dissemination of scientific research documents, whether they are published or not. The documents may come from teaching and research institutions in France or abroad, or from public or private research centers.

L'archive ouverte pluridisciplinaire **HAL**, est destinée au dépôt et à la diffusion de documents scientifiques de niveau recherche, publiés ou non, émanant des établissements d'enseignement et de recherche français ou étrangers, des laboratoires publics ou privés.

# Optimal description of Blaschke–Santaló diagrams via numerical shape optimization

Ilias Ftouhi

April 19, 2022

## Abstract

In this paper, we propose a method based on the combination of theoretical results on Blaschke–Santaló diagrams and numerical shape optimization techniques to obtain optimal description of Blaschke–Santaló diagrams in the class of convex sets. To illustrate our approach, we study three relevant diagrams involving the perimeter  $P$ , the diameter  $d$ , the volume  $|\cdot|$  and the first eigenvalue of the Laplace operator with Dirichlet boundary condition  $\lambda_1$ . The first diagram is a purely geometric one involving the triplet  $(P, d, |\cdot|)$  and the two other diagrams involve geometric and spectral functionals, namely  $(P, \lambda_1, |\cdot|)$  (studied in [1, 24]) and  $(d, \lambda_1, |\cdot|)$  where a strange phenomenon of non-continuity of the extremal shapes is observed.

## 1 Introduction

A Blaschke–Santaló diagram is a tool that allows to visualize all possible inequalities relating three quantities depending on the shape of a set: it was named as a reference to the works of W. Blaschke [9] and L. Santaló [44], where the authors were looking for the description of inequalities involving three geometrical quantities for a given convex set. Afterward, these diagrams have been extensively studied especially for the class of convex sets and more recently for triplets involving geometric and spectral functionals. For various examples on purely geometric functionals, we refer to the following non-exhaustive list of works [11, 12, 13, 20, 21, 22, 23, 29, 30, 31, 32, 33], and for examples involving both geometric and spectral quantities, we refer to [1, 2, 14, 16, 17, 24, 39, 48].

Let us first give an abstract setting for Blaschke–Santaló diagrams. We consider  $\mathcal{F}$  a class of subsets of  $\mathbb{R}^n$ ,  $n \geq 2$  and  $J_i : \Omega \in \mathcal{F} \mapsto J_i(\Omega) \in \mathbb{R}$ , where  $i \in \{1, 2, 3\}$  three homogenous shape functionals (i.e., for every  $i \in \{1, 2, 3\}$  there exists  $\alpha_i \in \mathbb{R}$  such that  $J_i(t\Omega) = t^{\alpha_i} J_i(\Omega)$  for  $t > 0$  and  $\Omega \in \mathcal{F}$ ). Several definitions of Blaschke–Santaló diagrams can be found in the literature, Thanks to the homogeneity properties of the functionals, we can adopt the following one:

**Definition 1.** *The Blaschke–Santaló diagram of the triplet  $(J_1, J_2, J_3)$  for the class  $\mathcal{F}$  is given by the following set:*

$$\mathcal{D} := \{(J_1(\Omega), J_2(\Omega)) \mid \Omega \in \mathcal{F} \text{ and } J_3(\Omega) = 1\}.$$

In the present paper, we are interested in the class  $\mathcal{K}$  of planar non-empty convex sets. We develop an approach based on the combination of theoretical and numerical results to provide an optimal description of Blaschke–Santaló diagrams. We recall that a complete description of such diagrams is equivalent to finding all the possible inequalities relating the involved functionals. Unfortunately, such analytical description can be quite difficult to obtain, especially when spectral functionals are involved, see for example [24, Conjecture 1] and the discussion therein. Thus, it is interesting to develop numerical tools that allow to obtain approximations of Blaschke–Santaló diagrams, which will surely help to develop the intuition and state some interesting conjectures. A natural idea is to generate a large number of random convex sets (more precisely convex polygons) for each we compute the involved functionals. Even if this process allows to obtain a cloud of dots that approaches the diagram, the results are not quite optimal since it is observed that some regions of the diagrams (those corresponding to smooth shapes) are quite sparse. We refer to [1], [24, Section 3.1] and [39, Section 5.3] for some examples.

In the present paper, we propose to combine a theoretical result of vertical convexity of the diagrams (see Theorem 2) with the obtained numerical solutions of some relevant shape optimization problems to provide an optimal approximation of the diagrams which allows to considerably improve the one obtained by the process of random generation of convex polygons, see Section 4 and the figures therein. We illustrate our strategy by applying it to diagrams involving the perimeter  $P$ , the diameter  $d$ , the volume  $|\cdot|$  and the first Dirichlet eigenvalue of the Laplacian  $\lambda_1$  defined as follows

$$\lambda_1(\Omega) := \min \left\{ \frac{\int_{\Omega} |\nabla u|^2 dx}{\int_{\Omega} u^2 dx}, u \in H_0^1(\Omega) \setminus \{0\} \right\},$$

where  $H_0^1(\Omega)$  denotes the completion for the  $H^1$ -norm of the space  $C_c^\infty(\Omega)$  of infinitely differentiable functions of compact support in  $\Omega$ , even though our strategy can be applied to many other examples.

More precisely, we study the following diagrams:

- The purely geometric diagram  $\mathcal{D}_1$  corresponding to the triplet  $(P, |\cdot|, d)$ :

$$\mathcal{D}_1 := \{(P(\Omega), |\Omega|) \mid \Omega \text{ is convex and } d(\Omega) = 1\}. \quad (1)$$

Up to our knowledge  $\mathcal{D}_1$  is not completely characterized yet, even though, several partial (but advanced) results are known, see [35, 41].

- The diagram  $\mathcal{D}_2$  corresponding to the triplet  $(P, \lambda_1, |\cdot|)$ :

$$\mathcal{D}_2 := \{(P(\Omega), \lambda_1(\Omega)) \mid \Omega \text{ is convex and } |\Omega| = 1\}, \quad (2)$$

that has been introduced for the first time in [1] and extensively studied in [24].

- The diagram  $\mathcal{D}_3$  corresponding to the triplet  $(d, \lambda_1, |\cdot|)$ :

$$\mathcal{D}_3 := \{(d(\Omega), \lambda_1(\Omega)) \mid \Omega \text{ is convex and } |\Omega| = 1\}. \quad (3)$$

This diagram has not yet been considered in the literature and we deemed it necessary to consider it since a strange phenomenon of non-continuity of the extremal shapes is observed, see Section 4.3 and more precisely Figure 20.

Let us state the following theoretical result:

**Theorem 2.** *The diagrams  $\mathcal{D}_1$ ,  $\mathcal{D}_2$  and  $\mathcal{D}_3$  are vertically convex, which means that if two points  $A(x, y_A)$  and  $B(x, y_B)$  belong to a diagram, then the (vertical) segment  $[AB]$  also belongs to the diagram.*

Once such a vertical convexity result is known, to obtain an optimal approximation of the diagram it is sufficient to numerically solve the following shape optimization problems:

$$\min / \max \{(J_1(\Omega) \mid \Omega \text{ is convex, } J_2(\Omega) = c_0 \text{ and } J_3(\Omega) = 1\}, \quad (4)$$

where  $J_1$ ,  $J_2$  and  $J_3$  are the involved shape functionals and  $c_0 > 0$  is a positive constant.

The convexity constraint allows in general to prove the existence of optimal shapes for problems of the type (4) (the proof is classical and relies on the standard method of calculus of variations). Such optimal shapes may be smooth or singular (polygonal for example), see for example [5, 19, 36, 37, 38]. This makes these kind of problems very interesting from a numerical point of view as one has to adapt the choice of the parametrization for each problem depending on the expected regularity of the solution. In the present paper, we present various (classical and one original) methods of parametrization that allow to handle the convexity constraint. We apply these techniques for the diagrams  $\mathcal{D}_1$ ,  $\mathcal{D}_2$  and  $\mathcal{D}_3$  and obtain satisfying results, see Section 4 and the figures therein.

The paper is organized as follows: Section 2 is devoted to the proof of Theorem 2, we also present and prove some interesting results on the diagram  $\mathcal{D}_3$  that has (up to our knowledge) never been considered in the literature, see Section 4.3. In Section 3, we present and review four parametrizations used to handle the convexity constraint and solve problems of the type (4). Three of these parametrizations are quite classical, this is the case of the ones based on the support functions (Section (3.1)), on the gauge function (Section (3.2)), see [4, 6, 10] and on the vertices of polygonal approximations of the sets (Section (3.3)), see [5], and the last one based on the radial function (Section (3.4)), which is up to our knowledge quite original as we did not manage to find a work where the convexity of the sets is modeled via some quadratic inequality constraints as in (11). In Section 4, we present the obtained optimal descriptions of the diagrams  $\mathcal{D}_1$ ,  $\mathcal{D}_2$  and  $\mathcal{D}_3$ . Finally, in Appendix, we compute the shape derivative of the diameter that is successfully implemented and used in our numerical simulations.

## 2 Proof of Theorem 2 and some theoretical results

The diagram  $\mathcal{D}_2$  has been studied in detail in [24], in particular Theorem 2 is already known for  $\mathcal{D}_2$ , we then focus on the diagrams  $\mathcal{D}_1$  and  $\mathcal{D}_3$ .

## 2.1 Some classical definitions and results of convex geometry

Before stating the proofs, we recall some classical definitions and results of convex geometry that we use in our proofs. Since in the present paper we are interested in the planar case, the definitions and propositions are stated in dimension 2, for a more general presentation and other results, we refer the reader to [45].

**Definition 3.** Let  $A$  and  $B$  be two subsets of  $\mathbb{R}^2$  and  $t > 0$ , we define

- the Minkowski sum of the sets  $A$  and  $B$  by

$$A \oplus B := \{x + y \mid x \in A \text{ and } y \in B\},$$

- and the dilatation of the set  $A$  by the positive coefficient  $t$  by

$$tA := \{tx \mid x \in A\}.$$

**Proposition 4** (Steiner formula [47]). Let  $\Omega$  be a planar convex body and  $B_1$  a ball of unit radius. We have

$$|\Omega + tB_1| = |\Omega| + tP(\Omega) + |B_1|t^2.$$

## 2.2 Proof of Theorem 2 for the diagram $\mathcal{D}_1$

We recall that

$$\mathcal{D}_1 := \{(P(\Omega), |\Omega|) \mid \Omega \text{ is convex and } d(\Omega) = 1\}.$$

Since in this case two of the involved functionals are linear with respect to the Minkowski sums and dilatation, the proof of the vertical convexity is quite standard. Let us consider two convex bodies  $K_0$  and  $K_1$  such that  $d(K_0) = d(K_1) = 1$  and  $P(K_0) = P(K_1) = p_0$ . For every  $t \in [0, 1]$ , we define

$$K_t = (1 - t)K_0 + tK_1.$$

Since the involved functionals are invariant by rotations, we assume without loss of generality that the diameters of  $K_0$  and  $K_1$  are colinear. We then have for every  $t \in [0, 1]$ ,

$$d(K_t) = (1 - t)d(K_0) + td(K_1) = (1 - t) + t = 1$$

and

$$P(K_t) = (1 - t)P(K_0) + tP(K_1) = (1 - t)p_0 + tp_0 = p_0.$$

Thus, by the continuity of the area with respect to the Hausdorff distance, the set  $\{(d(K_t), |K_t|) \mid t \in [0, 1]\}$  (which is included in the diagram  $\mathcal{D}_1$ ) contains the vertical segment connecting the points  $(p_0, |K_0|)$  and  $(p_0, |K_1|)$ , which proves the vertical convexity of the diagram.

## 2.3 The diagram $\mathcal{D}_3$

Unlikely for  $\mathcal{D}_1$ , the diagram  $\mathcal{D}_3$  does not involve two functionals that are linear with respect to the Minkowski sums and dilatation. This makes the strategy used in Section 2.2 impossible to adopt. The idea here is to adapt the strategy introduced and developed in [24] for the diagram  $\mathcal{D}_2$  involving the triplet  $(P, \lambda_1, |\cdot|)$  to the case of the triplet  $(d, \lambda_1, |\cdot|)$ .

### 2.3.1 Statement of the main results and proofs

We denote by  $B$  a ball of unit volume. We have

$$\mathcal{D}_3 := \{(d(\Omega), \lambda_1(\Omega)) \mid \Omega \text{ is convex and } |\Omega| = 1\} \subset [d(B), +\infty) \times [\lambda_1(B), +\infty),$$

where the inclusion is a consequence of the isodiametric inequality  $\frac{d(\Omega)}{\sqrt{\Omega}} \geq \frac{d(B)}{\sqrt{B}}$  and the Faber–Krahn inequality  $|\Omega|\lambda_1(\Omega) \geq |B|\lambda_1(B)$ .

Following the same strategy as in [24, Section 3.2], we introduce the functions

$$f : \begin{array}{ll} [d(B), +\infty) & \longrightarrow \mathbb{R} \\ x & \longmapsto \min \{\lambda_1(\Omega), \Omega \in \mathcal{K}, |\Omega| = 1 \text{ and } d(\Omega) = x\} \end{array} \quad (5)$$

$$g : \begin{array}{ll} [d(B), +\infty) & \longrightarrow \mathbb{R} \\ x & \longmapsto \max \{\lambda_1(\Omega), \Omega \in \mathcal{K}, |\Omega| = 1 \text{ and } d(\Omega) = x\} \end{array} \quad (6)$$

We have the following result:



**Theorem 5.** *The functions  $f$  and  $g$  are continuous and*

$$\mathcal{D}_3 = \{(x, y) \in \mathbb{R}^2, x \geq d(B) \text{ and } f(x) \leq y \leq g(x)\},$$

*which implies that the diagram  $\mathcal{D}_3$  is vertically convex. Moreover, the function  $f$  is strictly increasing.*

As explained in [24, Section 3.2.1], one main step in the proof of [24, Theorem 1.2] is the perturbation lemma [24, Lemma 3.5]. Indeed, once such result is shown, one can reproduce the same strategy of [24] and obtain the result stated in Theorem 5.

Let us state and show a perturbation lemma corresponding to the diagram  $\mathcal{D}_3$ :

**Lemma 6.** *(Perturbation Lemma) We denote by  $\mathcal{K}_1$  the class of planar convex bodies of unit volume endowed with the Hausdorff distance. We have*

1. *the ball is the only local minimizer of the diameter in  $\mathcal{K}_1$ .*
2. *There is no local maximizer of the perimeter in  $\mathcal{K}_1$ .*
3. *The ball is the only local minimizer of the  $\lambda_1$  in  $\mathcal{K}_1$ .*

*Proof.* 1. By the isodiametric inequality, the ball is the only global minimizer of the diameter in  $\mathcal{K}_1$  (it is then a local minimizer). We denote by  $B_1$  a ball of radius 1. Let us consider  $\Omega \in \mathcal{K}_1$  different from the ball. For every  $t \geq 0$ , we consider

$$\Omega_t := \frac{\Omega + tB_1}{\sqrt{|\Omega + tB_1|}} \in \mathcal{K}_1.$$

The sequence  $(\Omega_t)$  converges to  $\Omega$  with respect to the Hausdorff distance when  $t$  goes to 0 and we have

$$\begin{aligned} d(\Omega_t) &= d\left(\frac{\Omega + tB_1}{\sqrt{|\Omega + tB_1|}}\right) \\ &= \frac{d(\Omega) + 2t}{\sqrt{|\Omega + tB_1|}} \\ &= \frac{d(\Omega) + 2t}{\sqrt{|\Omega| + P(\Omega)t + \pi t^2}} \\ &= \frac{d(\Omega) + 2t}{\sqrt{1 + P(\Omega)t + \frac{o}{t \rightarrow 0^+}(t)}} \\ &= d(\Omega) + \frac{1}{2}(4 - P(\Omega)d(\Omega))t + \frac{o}{t \rightarrow 0^+}(t). \end{aligned}$$

Since  $\Omega$  is not a ball, we have  $4|\Omega| < P(\Omega)d(\Omega)$  (see [46] and the references therein). Thus,

$$4 - P(\Omega)d(\Omega) < 0.$$

This shows that the set  $\Omega$  is not a local minimizer of the diameter in  $\mathcal{K}_1$ .

2. Let us consider  $\Omega \in \mathcal{K}_1$ . Without loss of generality, we assume that a diameter of  $\Omega$  is colinear to the  $x$ -axis and contains the origin  $(0, 0)$ . We consider

$$a := \inf\{y \mid \exists x \in \mathbb{R}, (x, y) \in \Omega\} \text{ and } b := \sup\{y \mid \exists x \in \mathbb{R}, (x, y) \in \Omega\},$$

and for every  $t \in [0, 1)$ :

$$\Omega_t := \frac{\Omega \cap \{y \geq (1-t)a\} \cap \{y \leq (1-t)b\}}{\sqrt{|\Omega \cap \{y \geq (1-t)a\} \cap \{y \leq (1-t)b\}|}} \in \mathcal{K}_1.$$

We have for every  $t \in (0, 1)$

$$d(\Omega \cap \{y \geq (1-t)a\} \cap \{y \leq (1-t)b\}) = d(\Omega) \text{ and } |\Omega \cap \{y \geq (1-t)a\} \cap \{y \leq (1-t)b\}| < |\Omega| = 1,$$

thus

$$\forall t \in (0, 1), \quad d(\Omega_t) > d(\Omega).$$

Finally, since the sequence (of elements of  $\mathcal{K}_1$ )  $(\Omega_t)_{t \in (0, 1)}$  converges with respect to the Hausdorff distance to  $\Omega$ , the domain  $\Omega$  is not a local maximizer of the diameter in  $\mathcal{K}_1$ .

3. The last assertion is stated and proved in [24, Lemma 3.5].

□

Now, that a perturbation lemma is proved, it is straightforward to apply the same strategy in [24] by replacing the perimeter by the diameter. We note that as in the proof of [24, Theorem 3.9], the monotonicity of the function  $f$  is a consequence of the third assertion of Lemma 6.

### 2.3.2 A symmetry and regularity result

In this section, we prove a symmetry and regularity result on the domains that fill the lower boundary of the diagram  $\mathcal{D}_3$ , i.e., those solving the problem

$$\min\{\lambda_1(\Omega) \mid \Omega \subset \mathbb{R}^2 \text{ is convex, } d(\Omega) = d_0 \text{ and } |\Omega| = 1\}, \quad (7)$$

where  $d_0 > \frac{2}{\sqrt{\pi}}$  (we recall that if  $d_0 = \frac{2}{\sqrt{\pi}}$ , then, by the isodiametric inequality, the only solution of the problem is the ball).

Our result is stated as follows:

**Theorem 7.** *If  $\Omega^*$  is a solution of the problem (7), with  $d_0 > \frac{2}{\sqrt{\pi}}$ , then:*

1.  $\Omega^*$  admits two orthogonal axes of symmetry.
2. Apart from two diametrically opposed points (i.e., points of the boundary of the domain that are on opposite ends of a diameter), the boundary of  $\Omega^*$  is (at least)  $C^1$  at every point.

*Proof.* Let us prove each assertion:

1. Without loss of generality, we assume that there is a diameter of  $\Omega^*$  which is colinear to the  $x$ -axis and the origin  $(0, 0)$  is its midpoint. Let us prove that the  $x$  and  $y$  axis are two orthogonal axis of symmetry of  $\Omega^*$ . We argue by contradiction:

- if the  $x$ -axis is not an axis of symmetry of  $\Omega^*$ , we perform a continuous Steiner symmetrization (see [15] for example) with respect to the  $x$ -axis. It is well known that the volume and the convexity are preserved throughout this continuous process (see the proof of the second assertion of [24, Lemma 3.5] for the preservation of the convexity). Moreover, the diameter is also preserved by this process. Thus, by using the result of [18, Lemma 3.1], we deduce that this process strictly decreases the first Dirichlet eigenvalue of  $\Omega^*$  if it is not symmetric with respect to the  $x$ -axis.
- If the  $y$ -axis is not an axis of symmetry of  $\Omega^*$ , we use the same argument, but this time we symmetrize with respect to the  $y$ -axis. Here also, the volume, the diameter and the convexity are preserved, but the eigenvalue strictly decreases if the set  $\Omega^*$  is not symmetric with respect to the  $y$ -axis.

2. We recall that the lower boundary of the diagram  $\mathcal{D}_3$  is given by the graph of the function  $f$  defined in (5) as follows:

$$\begin{aligned} f : [d(B), +\infty) &\longrightarrow \mathbb{R} \\ x &\longmapsto \min\{\lambda_1(\Omega) \mid \Omega \in \mathcal{K}, |\Omega| = 1 \text{ and } d(\Omega) = x\} \end{aligned}$$

Let us assume, by contradiction, that  $\Omega^*$  has two distinct supporting lines at some point  $x_0$  of its boundary, such that there exist two diametrically opposed points both different from  $x_0$ . By removing a small cup as it is done in [28, Section 3.1] (see Figure 2 therein), we construct a family of convex sets  $(\Omega_\varepsilon)_{\varepsilon>0}$  converging with respect to the Hausdorff distance to  $\Omega^*$  when  $\varepsilon$  goes to  $0^+$ . By reproducing the same steps of the proof of [27, Lemma 3.3.2], we show that for sufficiently small values of  $\varepsilon > 0$ , we have the following points

- $|\Omega_\varepsilon| \lambda_1(\Omega_\varepsilon) < |\Omega^*| \lambda_1(\Omega^*) = \lambda_1(\Omega^*)$ .
- $|\Omega_\varepsilon| < |\Omega^*| = 1$  (because of the strict inclusion  $\Omega_\varepsilon \subset \Omega^*$ ).
- $d(\Omega_\varepsilon) = d(\Omega^*)$  (there exist two diametrically opposed points both different from  $x_0$ ).

Thus, by considering the normalized family  $\Omega_\varepsilon^* := \frac{\Omega_\varepsilon}{\sqrt{|\Omega_\varepsilon|}}$ , we dispose of a sequence of convex sets  $(\Omega_\varepsilon^*)$  of unit volume ( $|\Omega_\varepsilon^*| = 1$ ) converging to  $\Omega^*$  with respect to the Hausdorff distance such that

$$d(\Omega_\varepsilon^*) = d\left(\frac{\Omega_\varepsilon}{\sqrt{|\Omega_\varepsilon|}}\right) = \frac{d(\Omega_\varepsilon)}{\sqrt{|\Omega_\varepsilon|}} > \frac{d(\Omega^*)}{\sqrt{|\Omega^*|}} = d(\Omega^*),$$

and

$$f(d(\Omega_\varepsilon^*)) \leq \lambda_1(\Omega_\varepsilon^*) = \lambda_1\left(\frac{\Omega_\varepsilon}{\sqrt{|\Omega_\varepsilon|}}\right) = |\Omega_\varepsilon| \lambda_1(\Omega_\varepsilon) < \lambda_1(\Omega^*) = f(d(\Omega^*)).$$

Thus, we have

$$d(\Omega_\varepsilon^*) > d(\Omega^*) \text{ and } f(d(\Omega_\varepsilon^*)) < f(d(\Omega^*)),$$

which is a contradiction with the monotonicity of the function  $f$  proved in Theorem 5. This ends the proof of the regularity assertion.  $\square$

### 2.3.3 Further results and comments

We end this section by stating some interesting results and remarks:

- The result of monotonicity of the function  $f$  is quite interesting and useful as it yields the (non-trivial) equivalence between four shape optimization problems, as stated in the following corollary:

**Corollary 8.** *Let  $d_0 > d(B) = \frac{2}{\sqrt{\pi}}$ . The following problems are equivalent:*

1.  $\min\{\lambda_1(\Omega) \mid \Omega \in \mathcal{K}_1 \text{ and } d(\Omega) = d_0\}$
2.  $\min\{\lambda_1(\Omega) \mid \Omega \in \mathcal{K}_1 \text{ and } d(\Omega) \geq d_0\}$
3.  $\max\{d(\Omega) \mid \Omega \in \mathcal{K}_1 \text{ and } \lambda_1(\Omega) = f(p)\}$
4.  $\max\{d(\Omega) \mid \Omega \in \mathcal{K}_1 \text{ and } \lambda_1(\Omega) \leq f(p)\}$ ,

and, any solution satisfies the symmetry and regularity properties stated in Theorem 7.

The proof of this result is omitted as it is identical to the proof of [24, Corollary 3.13].

- We also note that the monotonicity of  $f$  is also used in the proof of the regularity result of Theorem 7.
- It is possible to obtain some sharp estimations on the functions  $f$  and  $g$  by using some classical inequalities. Indeed, we recall that by Makai's [40] and Polya's [42] inequalities, we have for every  $\Omega \in \mathcal{K}$

$$\frac{\pi^2}{16} \left( \frac{P(\Omega)}{|\Omega|} \right)^2 < \lambda_1(\Omega) < \frac{\pi^2}{4} \left( \frac{P(\Omega)}{|\Omega|} \right)^2. \quad (8)$$

Both estimates are sharp as the lower one is asymptotically attained by any family of thin vanishing triangles and the second one is asymptotically attained by any family of thin vanishing rectangles. By using the following inequalities

$$2d(\Omega) \leq P(\Omega) \leq \frac{|\Omega|}{d(\Omega)} + 2d(\Omega),$$

that are both sharp as the equality is asymptotically attained by any family of thin vanishing domains, see [46] and the references therein, we have

$$\frac{\pi^2}{4} \left( \frac{d(\Omega)}{|\Omega|} \right)^2 < \lambda_1(\Omega) < \frac{\pi^2}{4} \left( \frac{4\sqrt{|\Omega|}}{d(\Omega)} + \frac{2d(\Omega)}{\sqrt{|\Omega|}} \right)^2, \quad (9)$$

where both estimates are sharp as for (8). Finally, by using the definition of  $f$  and  $g$ , we have the following inequalities

$$\forall x \geq d(B) = \frac{2}{\sqrt{\pi}}, \quad \frac{\pi^2}{4} x^2 < f(x) \leq g(x) < \frac{\pi^2}{4} \left( \frac{4}{x} + 2x \right)^2.$$

Moreover, by the sharpness of the estimates 9, we have the following asymptotics

$$f(x) \underset{x \rightarrow +\infty}{\sim} \frac{\pi^2}{4} x^2 \text{ and } g(x) \underset{x \rightarrow +\infty}{\sim} \pi^2 x^2.$$

## 3 Parametrizations of convex sets and numerical setting

Before describing the parametrizations used in the present thesis, let us recall the definition of (directional) first order shape derivative that is very important in numerical shape optimization.

**Definition 9.** *let us take a shape depending functional  $J : \Omega \subset \mathbb{R}^n \rightarrow \mathbb{R}$ , where  $n \geq 2$ , and let  $V : \mathbb{R}^n \rightarrow \mathbb{R}^n$  a perturbation vector field. Let  $\Omega \subset \mathbb{R}^n$ , we take  $\Omega_t := (I + tV)(\Omega)$  where  $I : x \in \mathbb{R}^n \mapsto x$  is the identity map and  $t$  a sufficiently small positive number. We say that the functional  $J$  admits a directional shape derivative at  $\Omega$  in the direction  $V$  if the following limit  $\lim_{t \rightarrow 0^+} \frac{J(\Omega_t) - J(\Omega)}{t}$  exists. In this case we write*

$$J'(\Omega, V) := \lim_{t \rightarrow 0^+} \frac{J(\Omega_t) - J(\Omega)}{t}.$$

Now, let us present the four parametrizations considered in the paper and show how the convexity and the other constraints are implemented.

### 3.1 Parametrization via the support function

#### 3.1.1 Definitions and main properties

The support function is a useful tool to parametrize a convex set by a function defined on the unit sphere, it allows to turn geometrical problem into analytical problems and thus use tools from calculus of variations to solve geometrical problems, we refer for example to [26] for an analytical proof of the classical Blaschke-Lebesgue Theorem which states that among all planar convex domains of given constant width the Reuleaux triangle has minimal area and to [8, 25] for more examples.

Let us now recall the definition of the support function:

**Definition 10.** Let  $\Omega \in \mathcal{K}$  be a convex body (where  $n \geq 2$ ). The support function  $h_\Omega$  is defined on  $\mathbb{R}^n$  by:

$$\forall x \in \mathbb{R}^n, \quad h_\Omega(x) := \sup_{y \in \Omega} \langle x, y \rangle.$$

The support function is positively 1-homogeneous, so one can equivalently consider the restriction of  $h_\Omega$  to the unit sphere  $\mathbb{S}^{n-1}$ .

The support function has various interesting properties as linearity for Minkowski sums, characterizing a convex set and quite practical formulations of different geometrical quantities as the perimeter, diameter, area and width. There are many other properties that enhance the popularity of this parametrization, we refer to [45, Section 1.7.1] for a complete survey and detailed proofs.

Let us state the main properties of the support function used in the present thesis.

**Proposition 11.** Let  $\Omega_1, \Omega_2 \in \mathcal{K}$  and  $h_{\Omega_1}, h_{\Omega_2}$  the corresponding support functions, we have the following properties:

1.  $\Omega_1 = \Omega_2 \iff h_{\Omega_1} = h_{\Omega_2}$ .
2. If  $\Omega_1 \subset \Omega_2$ , then  $h_{\Omega_1} \leq h_{\Omega_2}$ .
3.  $h_{\Omega_1 \cap \Omega_2} = \min(h_{\Omega_1}, h_{\Omega_2})$ .
4.  $h_{\lambda_1 \Omega_1 + \lambda_2 \Omega_2} = \lambda_1 h_{\Omega_1} + \lambda_2 h_{\Omega_2}$ , where  $\lambda_1, \lambda_2 > 0$ .
5.  $d^H(\Omega_1, \Omega_2) = \|h_{\Omega_1} - h_{\Omega_2}\|_\infty := \sup_{u \in \mathbb{S}^{n-1}} |h_{\Omega_1}(u) - h_{\Omega_2}(u)|$ .

Since we are interested in the case of planar convex sets, from now on the support function of a set  $\Omega \in \mathcal{K}$  is defined by:

$$\forall \theta \in \mathbb{R}, \quad h_\Omega(\theta) = \sup_{x \in \Omega} \left\langle x, \begin{pmatrix} \cos \theta \\ \sin \theta \end{pmatrix} \right\rangle = \sup_{(x_1, x_2) \in \Omega} (x_1 \cos \theta + x_2 \sin \theta).$$

It is now natural to wonder how can the support function describe a convex shape (or more precisely its boundary). The following Proposition provides an efficient parametrization of strictly convex planar domains, which are considered in numerical simulations to approach the optimal shapes.

**Proposition 12.** Let  $\Omega \in \mathcal{K}$ . The support function  $h_\Omega$  of the convex  $\Omega$  is of class  $C^1$  on  $\mathbb{R}$  if and only if  $\Omega$  is strictly convex, in which case its boundary  $\partial\Omega$  will be parametrized as follows:

$$\begin{cases} x_\theta = h_\Omega(\theta) \cos \theta - h'_\Omega(\theta) \sin \theta, \\ y_\theta = h_\Omega(\theta) \sin \theta + h'_\Omega(\theta) \cos \theta, \end{cases}$$

where  $\theta \in [0, 2\pi]$ .

Now that we know that for any convex set one can associate a support function, it is natural to seek for conditions that a function should satisfy in order to be the support function of a convex set. The answer is tightly related to the fact that the convexity of a set is equivalent to the positivity of the radius of curvature at any point of its boundary.

**Proposition 13.** Let  $\Omega$  a strictly convex planar set, we assume that its support function  $h_\Omega$  is  $C^{1,1}$ , then the geometric radius of curvature of  $\partial\Omega$  is given by  $R_\Omega = h''_\Omega + h_\Omega$  and we have

$$\forall \theta \in [0, 2\pi], \quad R_\Omega(\theta) = h''_\Omega(\theta) + h_\Omega(\theta) \geq 0. \quad (10)$$

Reciprocally, if  $h$  is a  $C^{1,1}$ ,  $2\pi$  periodic function satisfying 10, then there exists a convex set  $\Omega \in \mathcal{K}$  such that  $h = h_\Omega$ .

**Remark 14.** *The results above are stated for strictly convex sets with smooth support functions (which is enough for the numerical simulations, see 3.1.2). Nevertheless, let us give some remarks on the singular cases:*

- *When  $h$  is just  $C^1$ , the condition  $R := h'' + h \geq 0$  can be understood in the sense of distributions that is to say that  $R := h'' + h$  is a positive Radon measure (i.e. for all  $C^\infty$  positive function  $\phi$  of compact support in  $[0, 2\pi]$ , one has:  $\int_0^{2\pi} R\phi \geq 0$ ).*
- *When  $\Omega$  is not strictly convex, the support function  $h_\Omega$  is not  $C^1$  and the measure corresponding to the radius of curvature  $R_\Omega$  may involve Dirac measures. This is for example the case for polygons where  $R_\Omega$  will be given by a finite sum of Dirac measures, see [45] for example.*

In addition to providing a quite simple description to the convexity constraint (see (10)), the support function provides elegant expressions for some relevant geometric functionals.

**Proposition 15.** *Let  $\Omega \in \mathcal{K}$  and  $h_\Omega$  its support function, we have the following formulas:*

1. *for the perimeter*

$$P(\Omega) = \int_0^{2\pi} h_\Omega(\theta) d\theta,$$

2. *for the minimal width*

$$w(\Omega) = \min_{\theta \in [0, 2\pi)} (h_\Omega(\theta) + h_\Omega(\pi + \theta)),$$

3. *for the diameter*

$$d(\Omega) = \max_{\theta \in [0, 2\pi)} (h_\Omega(\theta) + h_\Omega(\pi + \theta)),$$

4. *for the area*

$$|\Omega| = \frac{1}{2} \int_0^{2\pi} (h_\Omega^2(\theta) - h_\Omega'^2(\theta)) d\theta.$$

### 3.1.2 Numerical setting

Let us take  $\Omega \in \mathcal{K}$ . Since  $h_\Omega$  is an  $H^1$ ,  $2\pi$ -periodic function, it admits a decomposition in Fourier series:

$$h_\Omega(\theta) = a_0 + \sum_{n=1}^{\infty} (a_n \cos n\theta + b_n \sin n\theta),$$

where  $(a_n)_n$  and  $(b_n)_n$  denote the Fourier coefficients defined by:

$$a_0 = \frac{1}{2\pi} \int_0^{2\pi} h_\Omega(\theta) d\theta$$

and

$$\forall n \in \mathbb{N}^*, \quad a_n = \frac{1}{\pi} \int_0^{2\pi} h_\Omega(\theta) \cos(n\theta) d\theta, \quad b_n = \frac{1}{\pi} \int_0^{2\pi} h_\Omega(\theta) \sin(n\theta) d\theta.$$

We can then express the area and perimeter via the latter coefficient as follows:

$$P(\Omega) = 2\pi a_0 \quad \text{and} \quad |\Omega| = \pi a_0^2 + \frac{\pi}{2} \sum_{k=1}^{\infty} (1 - k^2)(a_k^2 + b_k^2).$$

To retrieve a finite dimensional setting, the idea is to parametrize sets via Fourier coefficients of their support functions truncated at a certain order  $N \geq 1$ . Thus, we will look for solutions in the set:

$$\mathcal{H}_N := \left\{ \theta \mapsto a_0 + \sum_{k=1}^N (a_k \cos(k\theta) + b_k \sin(k\theta)) \mid a_0, \dots, a_N, b_1, \dots, b_N \in \mathbb{R} \right\}.$$

This approach is justified by the following approximation proposition:

**Proposition 16.** *([45, Section 3.4])*

*Let  $\Omega \in \mathcal{K}$  and  $\varepsilon > 0$ . Then there exists  $N_\varepsilon$  and  $\Omega_\varepsilon$  with support function  $h_{\Omega_\varepsilon} \in \mathcal{H}_{N_\varepsilon}$  such that  $d^H(\Omega, \Omega_\varepsilon) < \varepsilon$ .*

For more convergence results and application of this method for different problems, we refer to [4].

Let  $N \geq 1$ , we summarize the parametrizations of functionals and constraints:

- The set  $\Omega$  is parametrized via  $a_0, \dots, a_N, b_1, \dots, b_N$ .
- The convexity constraint is given by the condition  $h''_{\Omega} + h_{\Omega} \geq 0$  on  $[0, 2\pi)$ . In [6] the authors provide an exact characterization of this condition in terms of the Fourier coefficients, involving concepts from semidefinite programming. In [3] the author provides a discrete alternative of the convexity inequality which has the advantage of being linear in terms of the Fourier coefficients. We choose  $\theta_m = 2\pi m/M$  where  $m \in \llbracket 1, M \rrbracket$  for some positive integer  $M$  and we impose the inequalities  $h''_{\Omega}(\theta_m) + h_{\Omega}(\theta_m) \geq 0$  for  $m \in \llbracket 1, M \rrbracket$ . As already shown in [3] we obtain the following system of linear inequalities:

$$\begin{pmatrix} 1 & \alpha_{1,1} & \cdots & \alpha_{1,N} & \cdots & \beta_{1,1} & \cdots & \beta_{1,N} \\ \vdots & \vdots & \ddots & \vdots & \cdots & \vdots & \ddots & \vdots \\ 1 & \alpha_{N,1} & \cdots & \alpha_{N,N} & \cdots & \beta_{N,1} & \cdots & \beta_{N,N} \end{pmatrix} \begin{pmatrix} a_0 \\ a_1 \\ \vdots \\ a_N \\ b_1 \\ \vdots \\ b_N \end{pmatrix} \geq \begin{pmatrix} 0 \\ \vdots \\ 0 \end{pmatrix}$$

where  $\alpha_{m,k} = (1 - k^2) \cos(k\theta_m)$  and  $\beta_{m,k} = (1 - k^2) \sin(k\theta_m)$  for  $(m, k) \in \llbracket 1, M \rrbracket \times \llbracket 1, N \rrbracket$ .

- The perimeter constraint  $P(\Omega) = p_0$  is given by

$$2\pi a_0 = p_0.$$

- The area constraint  $|\Omega| = A_0$  is given by

$$\pi a_0^2 + \frac{\pi}{2} \sum_{k=1}^N (1 - k^2)(a_k^2 + b_k^2) = A_0.$$

- The diameter constraint  $d(\Omega) = d_0$  is equivalent to

$$\begin{cases} \forall \theta \in [0, 2\pi), & h_{\Omega}(\theta) + h_{\Omega}(\pi + \theta) \leq d_0, \\ \exists \theta_0 \in [0, 2\pi), & h_{\Omega}(\theta_0) + h_{\Omega}(\pi + \theta_0) = d_0, \end{cases}$$

again as for the convexity We choose  $\theta_m = 2\pi m/M$  where  $m \in \llbracket 1, M' \rrbracket$  for some positive integer  $M'$  and we impose the inequalities  $h_{\Omega}(\theta_m) + h_{\Omega}(\pi + \theta_m) \leq d_0$  for  $m \in \llbracket 1, M' \rrbracket$ , we also assume without loss of generality that  $h_{\Omega}(0) + h_{\Omega}(\pi) = d_0$  (because all functionals are invariant by rotations). All these conditions can be written in terms of  $(a_k)$  and  $(b_k)$  as the following linear constraints:

$$\begin{cases} \forall m \in \llbracket 1, M' \rrbracket, & 2a_0 + \sum_{k=1}^N ((1 + (-1)^k) \cos(k\theta_m) \times a_k + (1 + (-1)^k) \sin(k\theta_m) \times b_k) \leq d_0, \\ & 2a_0 + \sum_{k=1}^N (1 + (-1)^k) a_k = d_0. \end{cases}$$

### 3.1.3 Computation of the gradients

In order to have an efficient optimization algorithm, we compute the derivatives of the eigenvalue and the area in terms of the Fourier coefficients of the support function (while for the convexity, the diameter and the perimeter constraints no gradient computation is needed in this setting since these constraints are linear). To this aim, we first consider two types of perturbations, a cosine term and a sine term, namely two families of deformations  $(V_{a_k})$  and  $(V_{b_k})$  that respectively correspond to the perturbation of the coefficients  $(a_k)$  and  $(b_k)$  in the Fourier decomposition of the support function. As stated in Proposition 12, when  $\Omega$  is strictly convex, the support function provides a parametrization of its boundary  $\partial\Omega = \{(x_{\theta}, y_{\theta}) \mid \theta \in [0, 2\pi]\}$ ; then the perturbation fields  $(V_{a_k})$  and  $(V_{b_k})$  are explicitly given on the boundary of  $\Omega$  as follows:

$$\begin{cases} V_{a_k}(x_{\theta}, y_{\theta}) = (\cos(k\theta) \cos \theta + k \sin(k\theta) \sin \theta, \cos(k\theta) \sin \theta - k \sin(k\theta) \cos \theta), & \text{where } k \in \llbracket 0, N \rrbracket \\ V_{b_k}(x_{\theta}, y_{\theta}) = (\sin(k\theta) \cos \theta + k \cos(k\theta) \sin \theta, \sin(k\theta) \sin \theta - k \cos(k\theta) \cos \theta), & \text{where } k \in \llbracket 1, N \rrbracket \end{cases}$$

If we denote by  $\mathcal{A} : \Omega \mapsto |\Omega|$  the area functional, we have the following formulas for the shape derivatives of the functional  $\mathcal{A}$  in the directions  $(V_{a_k})$  and  $(V_{b_k})$ :

$$\begin{cases} \mathcal{A}'(\Omega, V_{a_0}) = 2\pi a_0 \\ \mathcal{A}'(\Omega, V_{a_k}) = \pi(1 - k^2)a_k, & \text{where } k \in \llbracket 1, N \rrbracket \\ \mathcal{A}'(\Omega, V_{b_k}) = \pi(1 - k^2)b_k, & \text{where } k \in \llbracket 1, N \rrbracket \end{cases}$$

As for the Dirichlet eigenvalue, we recall that when  $\Omega$  is convex (or sufficiently smooth), the shape derivative of  $\lambda_1$  in a direction  $V : \mathbb{R}^2 \rightarrow \mathbb{R}^2$  is given by the following formula:

$$\lambda_1'(\Omega, V) = - \int_{\partial\Omega} |\nabla u_1|^2(x_\theta, y_\theta) \langle V(x_\theta, y_\theta), n(x_\theta, y_\theta) \rangle d\sigma,$$

where  $n(x_\theta, y_\theta) = (\cos \theta, \sin \theta)$  stands for the exterior unit normal vector to  $\partial\Omega$ ,  $u_1 \in H_0^1(\Omega)$  corresponds to a normalized eigenfunction (i.e.  $\|u_1\|_2 = 1$ ) corresponding to the first eigenvalue  $\lambda_1(\Omega)$  and  $d\sigma = (h_\Omega'' + h_\Omega)(\theta)d\theta$ , we refer to [27, Section 2.5] for more details on shape derivatives of eigenvalues. It is then possible by a change of variables to write the directional shape derivatives of  $\lambda_1$  as an integral on  $[0, 2\pi]$  as follows:

$$\begin{cases} \lambda_1'(\Omega, V_{a_k}) = - \int_0^{2\pi} |\nabla u|^2(x_\theta, y_\theta) \cos(k\theta) (h_\Omega''(\theta) + h_\Omega(\theta)) d\theta, & \text{where } k \in \llbracket 0, N \rrbracket, \\ \lambda_1'(\Omega, V_{b_k}) = - \int_0^{2\pi} |\nabla u|^2(x_\theta, y_\theta) \sin(k\theta) (h_\Omega''(\theta) + h_\Omega(\theta)) d\theta, & \text{where } k \in \llbracket 1, N \rrbracket. \end{cases}$$

The computation of the integrals is done by using an order 1 trapezoidal quadrature.

## 3.2 Parametrization via the Gauge function

### 3.2.1 Definition and main properties

A classical way to parametrize starshaped open sets (in particular convex ones) is by using the so-called *gauge function*.

**Definition 17.** Let  $\Omega$  a bounded, open subset of  $\mathbb{R}^n$  (with  $n \geq 2$ ) starshaped with respect to the origin. The gauge function  $u_\Omega$  is defined on  $\mathbb{R}^n$  by:

$$\forall x \in \mathbb{R}^n, \quad u_\Omega(x) = \inf\{t > 0 \mid tx \in \Omega\}.$$

The gauge function is positively 1-homogeneous, so one can equivalently consider the restriction of  $u_\Omega$  to the unit sphere  $\mathbb{S}^{n-1}$ .

In the planar case ( $n = 2$ ), we use polar coordinates representation  $(r, \theta)$  for the domains, we then define the gauge function on  $\mathbb{R}$  as follows:

$$\forall \theta \in \mathbb{R}, \quad u_\Omega(\theta) = \inf \left\{ t > 0 \mid t \begin{pmatrix} \cos \theta \\ \sin \theta \end{pmatrix} \in \Omega \right\}.$$

The open set  $\Omega$  is then given by:

$$\Omega = \left\{ (r, \theta) \in [0, +\infty) \times \mathbb{R} \mid r < \frac{1}{u_\Omega(\theta)} \right\}.$$

The curvature of the boundary of  $\Omega$  is given by:

$$\kappa_\Omega = \frac{u_\Omega'' + u_\Omega}{\left(1 + \left(\frac{u_\Omega'}{u_\Omega}\right)^2\right)^{\frac{3}{2}}},$$

where the second order derivative is to be understood in the sense of distributions. Thus, as for the support function, the starshaped set  $\Omega \subset \mathbb{R}^2$  is convex if and only if:

$$u_\Omega'' + u_\Omega \geq 0.$$

Moreover, straight lines in  $\partial\Omega$  are parameterized by the set  $\{u_\Omega'' + u_\Omega = 0\}$ , and corners in the boundary are seen as Dirac masses in the measure  $u_\Omega'' + u_\Omega$ . For example, the gauge function of a polygon will be given by a finite sum of Dirac masses at angles parametrizing the corners.

Both the perimeter and area can be expressed via gauge function. Unfortunately, this is not the case for the diameter.

**Proposition 18.** *Let  $\Omega$  a planar set star-shaped with respect to the origin. We have the following formulae:*

1. for the perimeter

$$P(\Omega) = \int_0^{2\pi} \frac{\sqrt{u_\Omega^2 + u_\Omega'^2}}{u_\Omega^2} d\theta.$$

2. for the area

$$|\Omega| = \frac{1}{2} \int_0^{2\pi} \frac{d\theta}{u_\Omega^2}.$$

### 3.2.2 Numerical setting

Similarly to the case of support function, in the planar case, we can decompose its gauge function as a Fourier series:

$$u_\Omega(\theta) = a_0 + \sum_{k=1}^{\infty} (a_k \cos k\theta + b_k \sin k\theta),$$

where  $(a_n)_n$  and  $(b_n)_n$  denote the Fourier coefficients defined by:

$$a_0 = \frac{1}{2\pi} \int_0^{2\pi} u_\Omega(\theta) d\theta$$

and

$$\forall k \in \mathbb{N}^*, \quad a_k = \frac{1}{\pi} \int_0^{2\pi} u_\Omega(\theta) \cos(k\theta) d\theta, \quad b_k = \frac{1}{\pi} \int_0^{2\pi} u_\Omega(\theta) \sin(k\theta) d\theta.$$

Here also, we look for solutions among truncated functions given in the following space:

$$\mathcal{H}_N := \left\{ \theta \mapsto a_0 + \sum_{k=1}^N (a_k \cos(k\theta) + b_k \sin(k\theta)) \mid a_0, \dots, a_N, b_1, \dots, b_N \in \mathbb{R} \right\}.$$

In practice, the computation of the perimeter and the area is done by considering a uniform discretization  $\{\theta_k := \frac{2k\pi}{M} \mid k \in \llbracket 0, M-1 \rrbracket\}$  of the interval  $[0, 2\pi)$ , with  $M$  a positive integer (we take it equal to 200 for the applications). We then approach the domain  $\Omega$  by the polygon  $\Omega_M$  of vertices  $A_k \left( \frac{\cos \theta_k}{u_\Omega(\theta_k)}, \frac{\sin \theta_k}{u_\Omega(\theta_k)} \right)$ , where  $k \in \llbracket 0, M-1 \rrbracket$ . The functionals perimeter and area (given as integrals in Proposition 18) are then computed in terms of  $(a_k)$  and  $(b_k)$  by using an order 1 trapezoidal quadrature:

$$\left\{ \begin{array}{l} P(\Omega) \approx \frac{1}{M} \sum_{k=0}^{M-1} \frac{\sqrt{u_\Omega^2(\theta_k) + u_\Omega'^2(\theta_k)}}{u_\Omega^2(\theta_k)} = \frac{1}{M} \sum_{k=0}^{M-1} \frac{\sqrt{\left( a_0 + \sum_{p=1}^N (a_p \cos(p\theta_k) + b_p \sin(p\theta_k)) \right)^2 + \left( \sum_{p=1}^N (-pa_p \sin(p\theta_k) + pb_p \cos(p\theta_k)) \right)^2}}{\left( a_0 + \sum_{p=1}^N (a_p \cos(p\theta_k) + b_p \sin(p\theta_k)) \right)^2}, \\ |\Omega| \approx \frac{1}{M} \sum_{k=0}^{M-1} \frac{1}{u_\Omega^2(\theta_k)} = \frac{1}{M} \sum_{k=0}^{M-1} \frac{1}{\left( a_0 + \sum_{p=1}^N (a_p \cos(p\theta_k) + b_p \sin(p\theta_k)) \right)^2}. \end{array} \right.$$

Here also the convexity is parametrized as in the last section by linear inequalities involving the coefficients  $(a_k)$  and  $(b_k)$ .

### 3.2.3 Computation of the gradients

The shape gradients of the area and the perimeter are computed by differentiating the explicit formulae above with respect to the Fourier coefficients. As for the Dirichlet eigenvalue, one has to use the Hadamard formula:

$$\lambda_1'(\Omega, V) = - \int_{\partial\Omega} |\nabla u_1|^2 \langle V, n \rangle d\sigma,$$

where  $u_1 \in H_0^1(\Omega)$  is a normalized eigenfunction (i.e.  $\|u_1\|_2 = 1$ ) corresponding to  $\lambda_1(\Omega)$  and  $V$  is a perturbation field corresponding to the perturbation of a Fourier coefficient. Let us investigate the values of such perturbations on the boundary of  $\Omega$ : let  $\phi : \theta \in \mathbb{R} \mapsto v(\theta)$  a Lipschitz  $2\pi$ -periodic function, for sufficiently small values of  $t > 0$ , we write:

$$\frac{1}{u_\Omega + t\phi} = \frac{1}{u_\Omega} \left( 1 + t \frac{\phi}{u_\Omega} \right)^{-1} = \frac{1}{u_\Omega} \left( 1 - \frac{\phi}{u_\Omega} \cdot t + \frac{o}{t \rightarrow 0}(t) \right) = \frac{1}{u_\Omega} - \frac{\phi}{u_\Omega^2} \cdot t + \frac{o}{t \rightarrow 0}(t).$$



We deduce that perturbing the gauge function in a direction  $\phi$  corresponds to a perturbation field defined on the boundary  $\partial\Omega = \left\{ \left( \frac{\cos \theta}{u_\Omega(\theta)}, \frac{\sin \theta}{u_\Omega(\theta)} \right) \mid \theta \in [0, 2\pi] \right\}$  by:

$$\left( \frac{\cos \theta}{u_\Omega(\theta)}, \frac{\sin \theta}{u_\Omega(\theta)} \right) \in \partial\Omega \longmapsto -\frac{\phi(\theta)}{u_\Omega^3(\theta)} \begin{pmatrix} \cos(\theta) \\ \sin(\theta) \end{pmatrix} \in \mathbb{R}^2.$$

We then deduce that the perturbation fields corresponding to the perturbations of the coefficients  $(a_k)$  and  $(b_k)$  are given by:

$$\begin{cases} V_{a_k} \left( \frac{\cos \theta}{u_\Omega(\theta)}, \frac{\sin \theta}{u_\Omega(\theta)} \right) = -\frac{\cos(k\theta)}{u_\Omega^3(\theta)} \begin{pmatrix} \cos(\theta) \\ \sin(\theta) \end{pmatrix}, & \text{where } k \in \llbracket 0, N \rrbracket, \\ V_{b_k} \left( \frac{\cos \theta}{u_\Omega(\theta)}, \frac{\sin \theta}{u_\Omega(\theta)} \right) = -\frac{\sin(k\theta)}{u_\Omega^3(\theta)} \begin{pmatrix} \cos(\theta) \\ \sin(\theta) \end{pmatrix}, & \text{where } k \in \llbracket 1, N \rrbracket, \end{cases}$$

where  $\theta \in [0, 2\pi]$ .

Once the perturbation fields are known, we use the polygonal approximation  $\Omega_M$  (introduced above in Paragraph 3.2.2) of the domain  $\Omega$  to provide a numerical approximation of the shape gradient as follows:

$$\lambda'_1(\Omega, V) \approx -\sum_{k=0}^{M-1} |\nabla u_1|^2(x_{I_k}, y_{I_k}) \langle V(x_{I_k}, y_{I_k}), n_k \rangle d\sigma_k,$$

with the convention  $A_M := A_0$  and:

- $d\sigma_k = \sqrt{(x_{A_k} - x_{A_{k+1}})^2 + (y_{A_k} - y_{A_{k+1}})^2}$ ,
- $I_k$  is the middle of the segment  $[A_k A_{k+1}]$ .
- $n_k := \frac{1}{d\sigma_k} \begin{pmatrix} -(y_{A_k} - y_{A_{k+1}}) \\ x_{A_k} - x_{A_{k+1}} \end{pmatrix}$  is the exterior unit vector normal to the segment  $[A_k A_{k+1}]$ .

### 3.3 Polygonal approximation and parametrization via the vertices

In this section, we propose to parametrize a convex set via the coordinates  $(x_k, y_k)_{k \in \llbracket 0, M-1 \rrbracket}$  of the vertices  $A_k$  of a corresponding polygonal approximation denoted by  $\Omega_M$  (with  $M \geq 3$ ). We assume that the points  $(A_k)_{k \in \llbracket 0, M-1 \rrbracket}$  form in this order a simple polygon (that is a polygon that does not intersect itself and has no holes) and recall the conventions  $A_M := A_0$  and  $A_{-1} := A_{M-1}$ .

As for the previous cases, we have formulas for the involved geometrical quantities:

$$\begin{cases} P(\Omega_M) = \sum_{k=0}^{M-1} \sqrt{(x_{k+1} - x_k)^2 + (y_{k+1} - y_k)^2}, \\ |\Omega_M| = \frac{1}{2} \left| \sum_{k=0}^{M-1} x_k y_{k+1} - x_{k+1} y_k \right| \\ d(\Omega_M) = \max_{i,j} \sqrt{(x_i - x_j)^2 + (y_i - y_j)^2} \end{cases}$$

It is easily seen that  $\Omega_M$  is convex if and only if all the interior angles are less than or equal to  $\pi$ . By using the cross product, this, in turn, is equivalent to the following quadratic constraints:

$$(x_{k-1} - x_k)(y_{k+1} - y_k) - (y_{k-1} - y_k)(x_{k+1} - x_k) \leq 0,$$

for  $k \in \llbracket 0, M-1 \rrbracket$ , where we used the conventions  $x_0 := x_M$ ,  $y_0 := y_M$ ,  $x_{M+1} := x_1$  and  $y_{M+1} := y_1$ . This characterization of convexity is quite natural and has already been considered in literature, see [5] for example.

The gradients of the perimeter, area and convexity constraints (corresponding to the variables  $(x_k)$  and  $(y_k)$ ) are directly obtained by differentiating the explicit formulae given above. On the other hand, the gradients of the eigenvalue and diameter are computed (as in the last section) by using shape derivative formulae (see [27, Section 2.5] for  $\lambda_1$  and Theorem 21 for the diameter), where, we use the perturbation vector fields  $(V_{x_k})$  and  $(V_{y_k})$  corresponding to the variables  $(x_k)$  and  $(y_k)$ , see Figure 1.

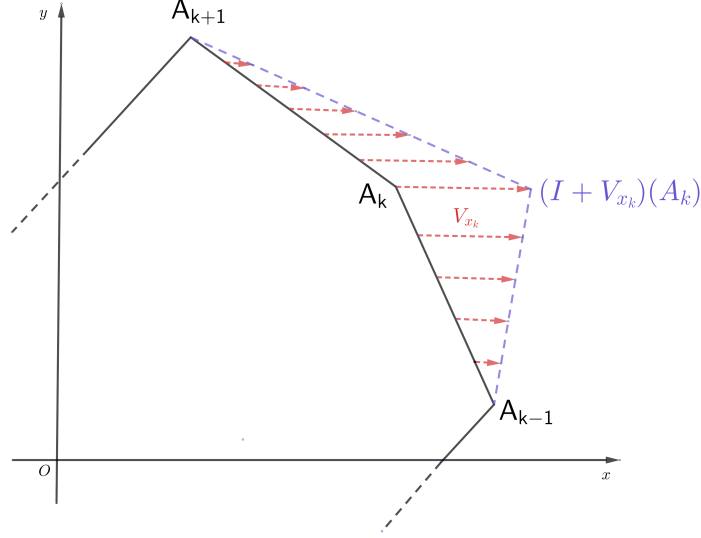


Figure 1: Perturbation field  $V_{x_k}$  associated to the parameter  $x_k$ .

### 3.4 Parametrization via the radial function

#### 3.4.1 Definition and main properties

It is common to parametrize star-shaped domains via their *radial function*. In this section, we present this parametrization

**Definition 19.** Let  $n \geq 2$  and  $\Omega \subset \mathbb{R}^n$  a domain star-shaped with respect to the origin. The radial function  $\rho_\Omega$  is defined on  $\mathbb{R}^n$  by:

$$\forall x \in \mathbb{R}^n, \quad \rho_\Omega(x) = \sup\{t > 0 \mid tx \in \Omega\}.$$

The radial function is positively 1-homogeneous, so one can equivalently consider the restriction of  $\rho_\Omega$  to the unit sphere  $\mathbb{S}^{n-1}$ .

In the planar case we can define the radial function on  $\mathbb{R}$  as follows:

$$\forall \theta \in \mathbb{R}, \quad \rho_\Omega(\theta) = \sup \left\{ t > 0 \mid t \begin{pmatrix} \cos \theta \\ \sin \theta \end{pmatrix} \in \Omega \right\}.$$

If  $\Omega \subset \mathbb{R}^2$  is open, it can be given in polar coordinates as follows:

$$\Omega = \{(r, \theta) \in [0; +\infty) \times \mathbb{R} \mid r < \rho_\Omega(\theta)\}.$$

We remark that the radial function is simply the inverse of the gauge function introduced before.

#### 3.4.2 Numerical setting

Unfortunately, in contrary to the previous cases, convexity cannot be given by linear constraints on the Fourier coefficients of the periodic function  $\rho_\Omega$ . We propose to approximate a set via polygons of vertices  $\rho_\Omega(\theta_k) \begin{pmatrix} \cos \frac{2k\pi}{M} \\ \sin \frac{2k\pi}{M} \end{pmatrix} \in \mathbb{R}^2$ , where  $k \in \llbracket 0, M-1 \rrbracket$  and  $M$  a sufficiently large integer (in practice we take  $M = 200$ ).

Thus, a star-shaped set  $\Omega$  will be parametrized via  $M$  positive distances  $(\rho_k)_{k \in \llbracket 1, M \rrbracket}$  that describe a polygonal approximation of  $\Omega$  given by vertices  $A_k = \rho_k \begin{pmatrix} \cos \frac{2k\pi}{M} \\ \sin \frac{2k\pi}{M} \end{pmatrix}$ . We always consider the convention  $A_M := A_0$  and  $A_{-1} := A_{M-1}$  (in particular  $\rho_M := \rho_0$  and  $\rho_{-1} := \rho_{M-1}$ ).

This setting allows to give good approximations of the involved geometrical functionals (perimeter, area and diameter). we have

1. for the area:

$$|\Omega| = \frac{1}{2} \sin \frac{2\pi}{M} \cdot \sum_{k=0}^{M-1} \rho_k \rho_{k+1},$$

2. for the perimeter:

$$P(\Omega) = \sum_{k=0}^{M-1} \sqrt{\rho_k^2 + \rho_{k+1}^2 - 2\rho_k\rho_{k+1} \cos\left(\frac{2k\pi}{M}\right)},$$

3. and the diameter:

$$d(\Omega) = \max_{i \neq j} \sqrt{\left[\rho_i \cos \frac{2i\pi}{M} - \rho_j \cos \frac{2j\pi}{M}\right]^2 + \left[\rho_i \sin \frac{2i\pi}{M} - \rho_j \sin \frac{2j\pi}{M}\right]^2},$$

this formula provides the diameter in  $\mathcal{O}(M^2)$  complexity. When the polygon is convex we use a faster method of computation (with complexity  $\mathcal{O}(M)$ ), which consists of finding all antipodal pairs of points and looking for the diametrical between them. This is classically known as Shamos algorithm [43].

It remains to describe the convexity constraint via the parameters  $(\rho_k)_{k \in \llbracket 0, M-1 \rrbracket}$ : we remark that the polygon (which contains the origin  $O$ ) whose vertices are given by  $A_k := (\rho_k \cos \frac{2k\pi}{M}, \rho_k \sin \frac{2k\pi}{M})$  is convex if and only if the sum of the areas of the triangles  $OA_k A_{k+1}$  and  $OA_k A_{k-1}$  is less or equal than the area of  $OA_{k-1} A_{k+1}$ , see Figure 2.

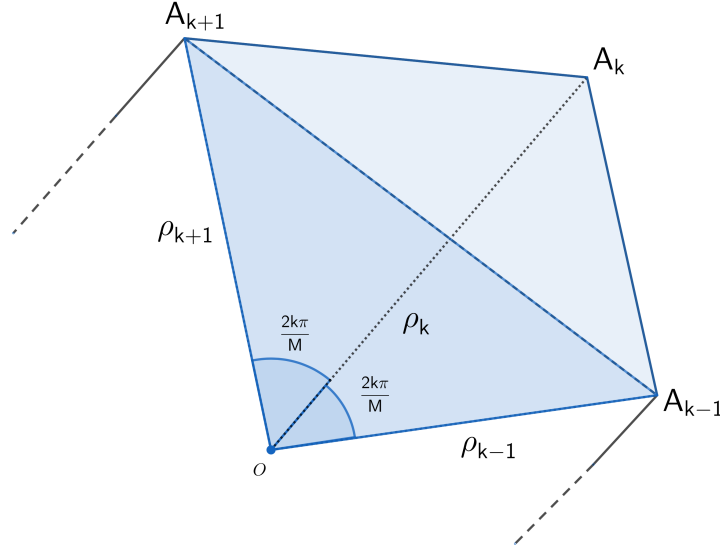


Figure 2: Convexity constraint via areas of the triangles.

We have

$$\begin{cases} \mathcal{S}_{OA_{k-1}A_k} = \frac{1}{2}\rho_{k-1}\rho_k \sin \frac{2k\pi}{M} \\ \mathcal{S}_{OA_kA_{k+1}} = \frac{1}{2}\rho_k\rho_{k+1} \sin \frac{2k\pi}{M} \\ \mathcal{S}_{OA_{k-1}A_{k+1}} = \frac{1}{2}\rho_{k-1}\rho_{k+1} \sin \frac{4k\pi}{M} = \rho_{k-1}\rho_{k+1} \sin \frac{2k\pi}{M} \cos \frac{2k\pi}{M}. \end{cases}$$

Thus, the convexity constraint given by  $\mathcal{S}_{OA_{k-1}A_k} + \mathcal{S}_{OA_kA_{k+1}} \geq \mathcal{S}_{OA_{k-1}A_{k+1}}$  is equivalent to the following quadratic constraint:

$$C_k := 2 \cos\left(\frac{2\pi}{M}\right) \rho_{k-1}\rho_{k+1} - \rho_k(\rho_{k-1} + \rho_{k+1}) \leq 0, \quad (11)$$

where  $k \in \llbracket 0, M-1 \rrbracket$ .

### 3.4.3 Computation of the gradients

Now that we brought the shape optimization problem to a finite dimensional optimization one, it remains to compute the gradients of the involved functionals and constraints.

Let us take  $\Omega \subset \mathbb{R}^2$  a domain whose starshaped with respect to the origin  $O$ , that we assume to be parametrized by  $(\rho_k)_{k \in \llbracket 0, M-1 \rrbracket}$ . For any  $k \in \llbracket 0, M-1 \rrbracket$  we denote by  $V_{\rho_k}$  the perturbation field corresponding to the perturbation of the variable  $\rho_k$ . It is null on the whole boundary except on the sides  $[A_{k-1}A_k]$  and  $[A_kA_{k+1}]$ , see Figure 3.

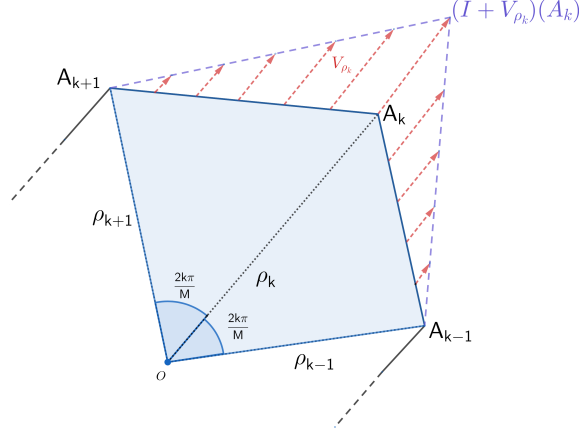


Figure 3: Perturbation field  $V_{\rho_k}$ .

Since we dispose of explicit formulae for the perimeter and the area, we can directly compute the corresponding shape gradients. We have for every  $k \in \llbracket 0, M-1 \rrbracket$ :

$$\mathcal{A}'(\Omega, V_{\rho_k}) = \frac{\sin\left(\frac{2\pi}{M}\right)}{2} \cdot (\rho_{k-1} + \rho_{k+1}),$$

and

$$P'(\Omega, V_{\rho_k}) = \frac{\rho_k - \rho_{k-1} \cos\left(\frac{2\pi}{M}\right)}{\sqrt{\rho_{k-1}^2 + \rho_k^2 - 2\rho_{k-1}\rho_k \cos\left(\frac{2\pi}{M}\right)}} + \frac{\rho_k - \rho_{k+1} \cos\left(\frac{2\pi}{M}\right)}{\sqrt{\rho_{k+1}^2 + \rho_k^2 - 2\rho_{k+1}\rho_k \cos\left(\frac{2\pi}{M}\right)}}.$$

For the eigenvalue, we use as before the Hadamard formula:

$$\lambda'_1(\Omega, V) = - \int_{\partial\Omega} |\nabla u_1|^2 \langle V, n \rangle d\sigma,$$

where  $u_1 \in H_0^1(\Omega)$  is a normalized eigenfunction (i.e.  $\|u_1\|_2 = 1$ ) corresponding to  $\lambda_1(\Omega)$  and  $V$  is a perturbation field.

For every  $k \in \llbracket 0, M-1 \rrbracket$ , we discretize the side  $[A_k A_{k+1}]$  in  $\ell$  small segments of length  $\frac{A_k A_{k+1}}{\ell}$  centered in some points  $B_k^i \in [A_k A_{k+1}]$ . We then compute approximations of the gradients as follows:

$$\lambda'_1(\Omega, V_{\rho_k}) \approx - \frac{1}{\ell} \sum_{i=1}^{\ell} (|\nabla u_1|^2(x_{B_k^i}, y_{B_k^i}) \langle V_{\rho_k}(x_{B_k^i}, y_{B_k^i}), n_k \rangle d\sigma_k - |\nabla u_1|^2(x_{B_{k-1}^i}, y_{B_{k-1}^i}) \langle V_{\rho_k}(x_{B_{k-1}^i}, y_{B_{k-1}^i}), n_{k-1} \rangle d\sigma_{k-1}),$$

with:

- the conventions  $A_M := A_0$  and  $A_{-1} := A_{M-1}$  (in particular  $\rho_M := \rho_0$  and  $\rho_{-1} := \rho_{M-1}$ ),
- the points  $(B_k^i)_{i \in \llbracket 1, \ell \rrbracket}$
- $d\sigma_k = \sqrt{(x_{A_k} - x_{A_{k+1}})^2 + (y_{A_k} - y_{A_{k+1}})^2}$ ,
- $\forall i \in \llbracket 1, \ell \rrbracket, \quad B_k^i := \left(1 - \frac{i}{\ell}\right) A_k + \frac{i}{\ell} A_{k+1}$ ,
- $n_k := \frac{1}{d\sigma_k} \begin{pmatrix} -(y_{A_k} - y_{A_{k+1}}) \\ x_{A_k} - x_{A_{k+1}} \end{pmatrix}$  is the exterior unit vector normal to the segment  $[A_k A_{k+1}]$ .

Finally, for the diameter, we use the following shape derivative formula obtained in Theorem 21:

$$d'(\Omega, V) = \max \left\{ \left\langle \frac{x-y}{|x-y|}, V(x) - V(y) \right\rangle \mid x, y \in \Omega, \text{ such that } |x-y| = d(\Omega) \right\}.$$

### 3.5 Computations of the functionals and numerical optimization

Let us give few words on the numerical computation of the functionals. In all the parametrizations above we dispose of analytical formulas that provide good approximations of the area and the perimeter. Let us give some elements on the computations of the remaining functionals involved in the paper:

- **the first Dirichlet eigenvalue** is computed by the "Partial Differential Equation Toolbox" of Matlab that is based on finite elements methods.
- As explained in the sections above, the computation of the diameter depends on the choice of the parametrization: indeed, when parameterizing a convex  $\Omega$  via its support function  $h_\Omega$ , it is given by  $d(\Omega) = \max_{\theta \in [0, 2\pi]} (h_\Omega(\theta) + h_\Omega(\pi + \theta))$ , meanwhile, when using a polygonal approximation, we compute the diameter of the convex hull via a fast method of computation (with complexity  $\mathcal{O}(M)$ , where  $M$  is the number of vertices), which consists of finding all antipodal pairs of points and looking for the diametrical between them. This is classically known as Shamos algorithm [43].

As for the optimization, we used Matlab's `fmincon` function with the `interior-point` and/or `sqp` algorithms.

## 4 Optimal numerical description of Blaschke–Santaló diagrams

In the present section, we show how the application of the different methods described in Section 3 can be used to obtain optimal descriptions of the boundaries of the diagrams  $\mathcal{D}_1$ ,  $\mathcal{D}_2$  and  $\mathcal{D}_3$  introduced in Section 1.

### 4.1 The diagram $\mathcal{D}_1$ of the triplet $(P, |\cdot|, d)$

#### 4.1.1 Naive approach and classical results

We are interested in studying the diagram

$$\mathcal{D}_1 := \{(P(\Omega), |\Omega|) \mid \Omega \in \mathcal{K} \text{ and } d(\Omega) = 1\}.$$

This diagram is (as far as we know) one of the unsolved diagrams introduced by Santaló in [44], but we note that there are quite advanced results on the characterization of its boundary:

- in [41], the authors solve the problem corresponding to the upper boundary, namely they prove that the problem

$$\max\{|\Omega| \mid \Omega \in \mathcal{K}, P(\Omega) = p_0 \text{ and } d(\Omega) = 1\},$$

where  $p_0 \in (2, \pi]$ , is solved by symmetric lenses (that are given by the intersection of two balls with the same radius) of diameter 1 and perimeter  $p_0$ .

- In [35], the author manages to describe the lower boundary of the diagram that corresponds to perimeters  $p_0 \in (2, 3]$ , he shows that the optimal domains are given by *subequilateral triangles* (ie. isosceles triangles whose smaller inner angle is less than  $\frac{\pi}{3}$ ).
- At last, there is the famous Blaschke–Lebesgue's Theorem, named after W. Blaschke and H. Lebesgue, which states that the Reuleaux triangle (see Figure 4) has the least area of all domains of given constant width. It is classical that sets of constant width have the same perimeter, thus in the diagram, those sets fill the vertical line  $\{\pi\} \times [\frac{1}{2}(\pi - \sqrt{3}), \frac{\pi}{4}]$ , see Figure 4.

As stated in Theorem 2 and proved in Section 2.2, the diagram is vertically convex.

In Figure 4, we plot the points corresponding to the extremal sets described above and a cloud of dots obtained by randomly generating  $10^5$  polygons whose numbers of sides are in  $[[3, 30]]$ .

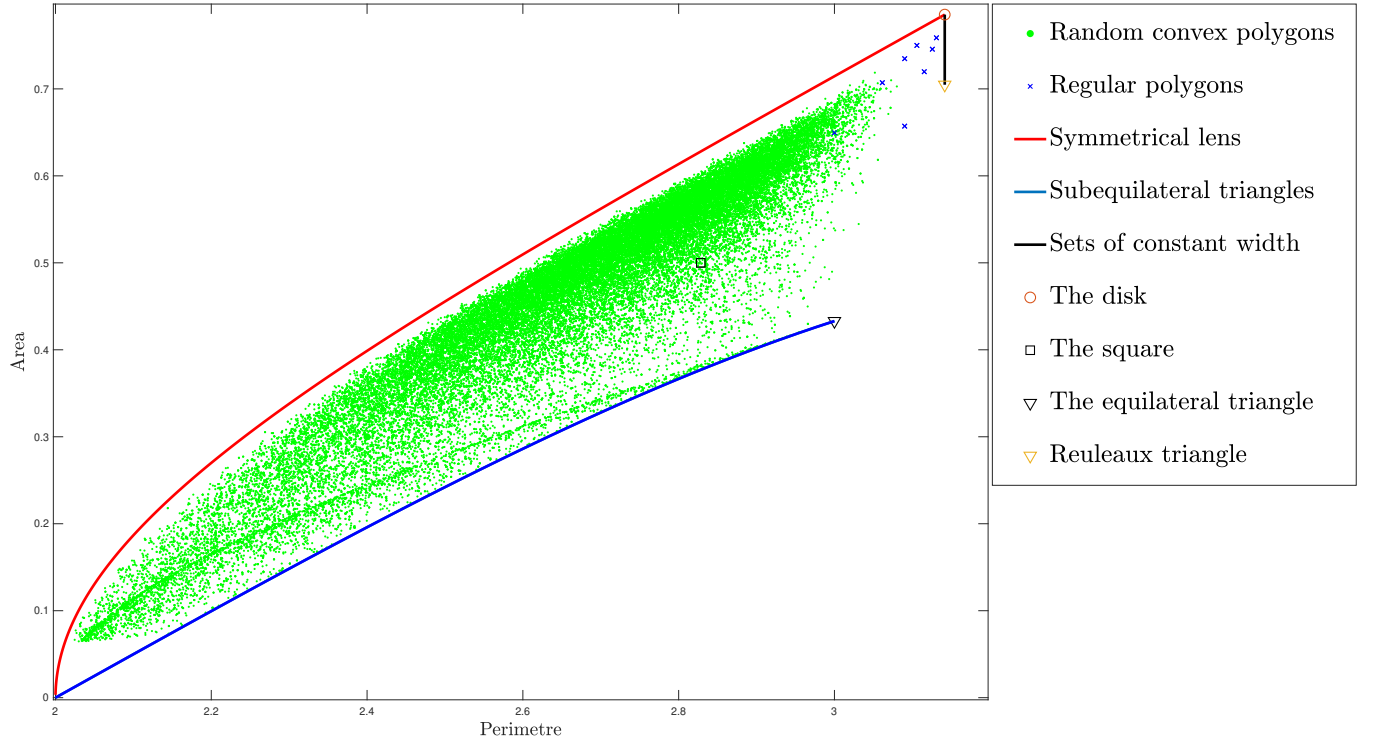


Figure 4: Approximation of the diagram  $\mathcal{D}_1$  via random convex sets and some relevant shapes.

#### 4.1.2 On the numerical approximation of the extremal shapes

We use the methods of Section 3, in order to obtain a numerical approximation of the missing boundary (which should be connecting the equilateral and Reuleaux triangles in Figure 4).

We numerically solve the following shape optimization problems:

$$\min \setminus \max\{|\Omega| \mid \Omega \in \mathcal{K}, P(\Omega) = p_0 \text{ and } d(\Omega) = 1\}, \quad (12)$$

where  $p_0 \in (3, \pi/4)$ .

The parametrization via the Fourier coefficients of the support function (Section 3.1) allows to obtain quite satisfying results as we obtain symmetrical lenses (see Figure 5) as optimal shapes (which is in concordance with the result proved in [41]).

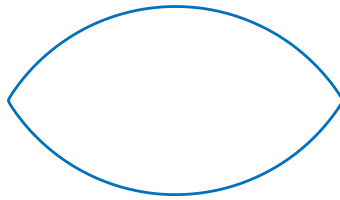


Figure 5: Symmetrical lens obtained as a solution of the problem  $\max\{|\Omega| \mid \Omega \in \mathcal{K}, P(\Omega) = 2.4 \text{ and } d(\Omega) = 1\}$ .

As for the lower boundary, to obtain good approximations, we combine the two methods of sections 3.1 and 3.4. We first use the parametrization via Fourier coefficients of the support function truncated at a certain order  $N$  to find first approximations of the extremal sets that will be used as initial shapes for the parametrization using radial function. We note that by this process we are able to obtain quite accurate description of the lower boundary, see Figure 10.

In a first time, as explained in section 3.1, by using the parametrization via the Fourier coefficients of the support

function, the Problem (12) is reduced to the following finite dimensional minimization problem:

$$\min_{(a_0, \dots, b_N) \in \mathbb{R}^{2N+1}} \left( \pi a_0^2 + \frac{\pi}{2} \sum_{k=1}^N (1 - k^2)(a_k^2 + b_k^2) \right),$$

with linear constraints on the Fourier coefficients:

- a perimeter constraint:  $2\pi a_0 = p_0$ ,
- and the convexity constraint:

$$\begin{pmatrix} 1 & \alpha_{1,1} & \cdots & \alpha_{1,N} & \cdots & \beta_{1,1} & \cdots & \beta_{1,N} \\ \vdots & \vdots & \ddots & \vdots & \cdots & \vdots & \ddots & \vdots \\ 1 & \alpha_{N,1} & \cdots & \alpha_{N,N} & \cdots & \beta_{N,1} & \cdots & \beta_{N,N} \end{pmatrix} \begin{pmatrix} a_0 \\ a_1 \\ \vdots \\ a_N \\ b_1 \\ \vdots \\ b_N \end{pmatrix} \geq \begin{pmatrix} 0 \\ \vdots \\ 0 \end{pmatrix}$$

where  $\alpha_{m,k} = (1 - k^2) \cos k\theta_m$  and  $\beta_{m,k} = (1 - k^2) \sin k\theta_m$  for  $(m, k) \in \llbracket 1, M \rrbracket \times \llbracket 1, N \rrbracket$ , with  $M$  taken to be equal to 1000.

Before showing the obtained results, let us first analyze the accuracy of the present method (based the support function): we solve the latter optimization problem for different values of the parameter  $N$  in the case  $p_0 = 3$  for which we know that the optimal shape is given by the equilateral triangle.

Here are the optimal shapes obtained for the choices of  $N \in \{20, 40, 100, 140\}$ :

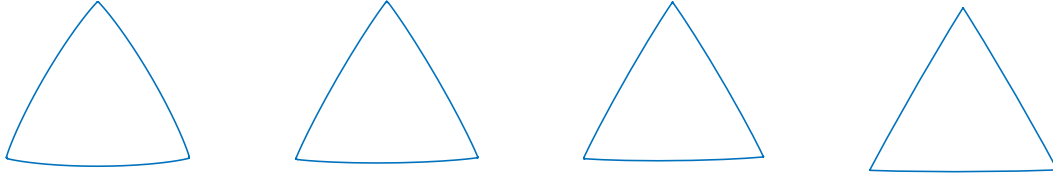


Figure 6: Obtained solutions for  $p_0 = 3$  and  $N \in \{20, 40, 100, 140\}$  (approximation of an equilateral triangle).

In the Figure 7, we plot the relative errors in function of the order of truncation  $N$ . It shows that the method based on the support function is not very relevant when the optimal shape is polygonal (which can frequently be the case when imposing convexity constraint).

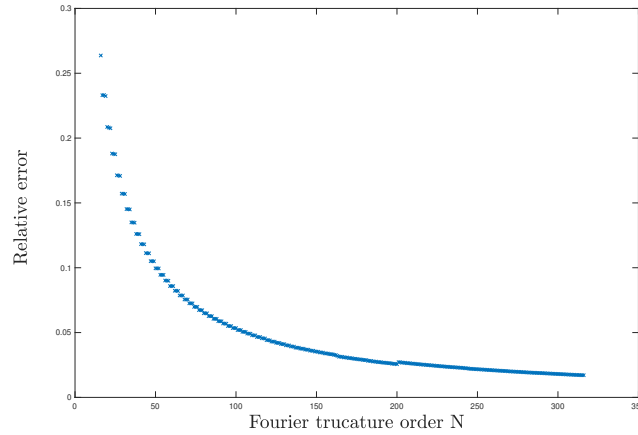


Figure 7: Relative errors in function of the truncation order  $N$  in the case  $p_0 = 3$ .

We then obtain (see Figure 8) an approximation of the missing lower boundary corresponding to domains obtained by considering 401 Fourier coefficients ( $N = 200$ ).

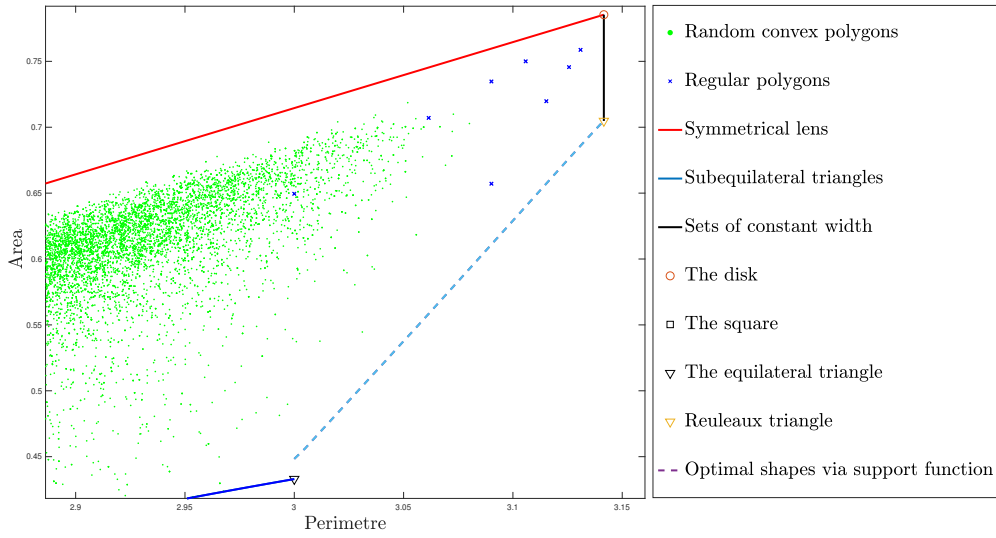


Figure 8: Approximation of the missing part of the lower boundary by optimizing the Fourier coefficients of the support function.

We then, use the obtained domains as initial shapes for the method based on the radial function (see Section 3.4) and find better shapes, which improves the description of the missing part in the lower boundary of the diagram  $\mathcal{D}_1$  (see Figures 9 and 10).

Method	Support function	Radial function
Obtained shape for $p_0 = 3.07$ in the minimization problem (12)		
Corresponding area	0.5881	0.5687

Figure 9: The radial function parametrization allows to improve the result of the support function method.

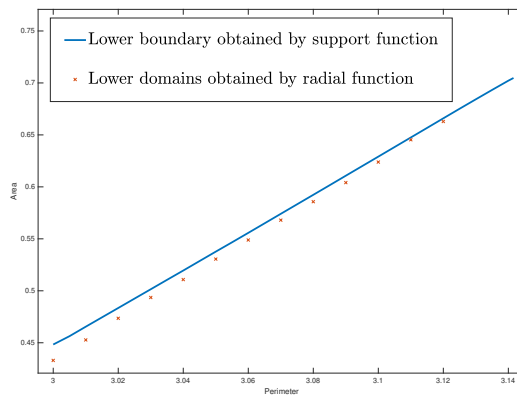


Figure 10: Improved description of the lower boundary by combining the two methods.



**Remark 20.** We refer to the recent work [10], where the author proposes an improvement of the methods based on the Fourier coefficients of the support and gauge functions of convex sets (described in sections 3.2 and 3.1), in such a way to tackle the issue related to the appearance of segments or corners in the optimal shape.

#### 4.1.3 Extremal shapes and improved description of the diagram

At last, we provide some extremal shapes obtained for relevant values of  $p_0$  in Figure 11 and improved description of the diagram  $\mathcal{D}_1$  in Figure 12.

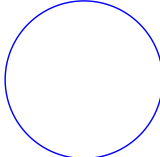
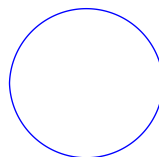
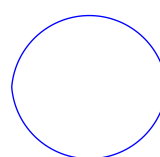
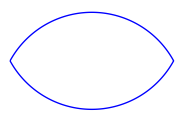
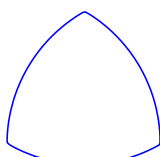
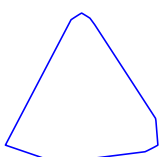
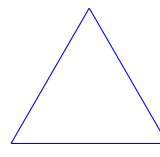
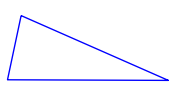
Problem	$p_0 = \pi$	$p_0 = 3.07$	$p_0 = 3$	$p_0 = 2.4$
Upper boundary				
Lower boundary				

Figure 11: Extremal shapes corresponding to different values of  $p_0$ .

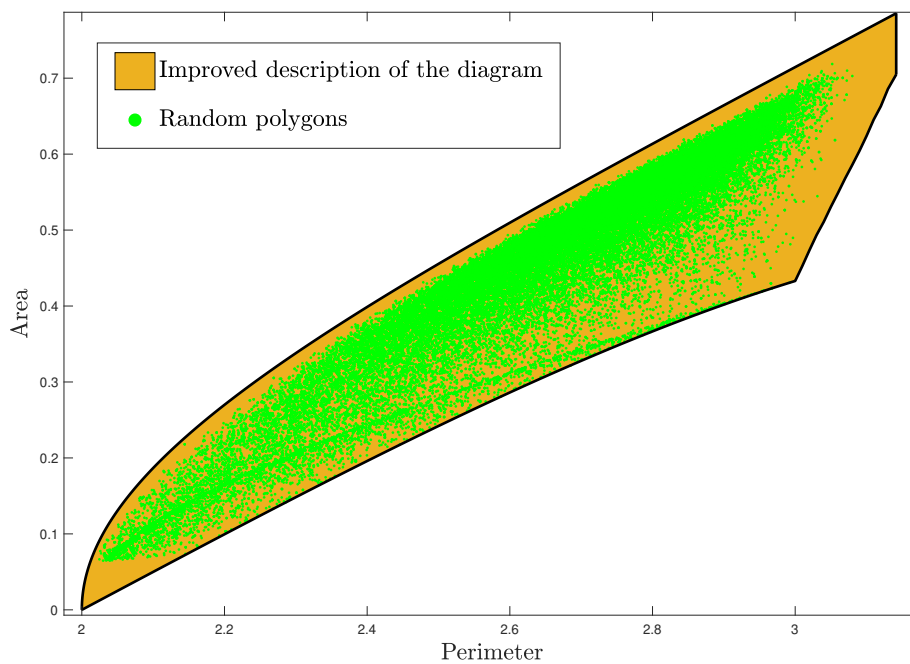


Figure 12: Improved description of the diagram of the triplet  $(P, |\cdot|, d)$ .

## 4.2 The diagram $\mathcal{D}_2$ of the triplet $(P, \lambda_1, |\cdot|)$

The diagram of the triplet  $(P, \lambda_1, |\cdot|)$  is given by

$$\mathcal{D}_2 := \{(P(\Omega), \lambda_1(\Omega)) \mid \Omega \in \mathcal{K} \text{ and } |\Omega| = 1\}.$$

This diagram has been first introduced by P. Antunes and P. Freitas in [1] and deeply investigated in [24].

In a first time, we give an approximation of the diagram by generating  $10^5$  random convex polygons (as it was done before in [1]). We obtain the following Figure 13:

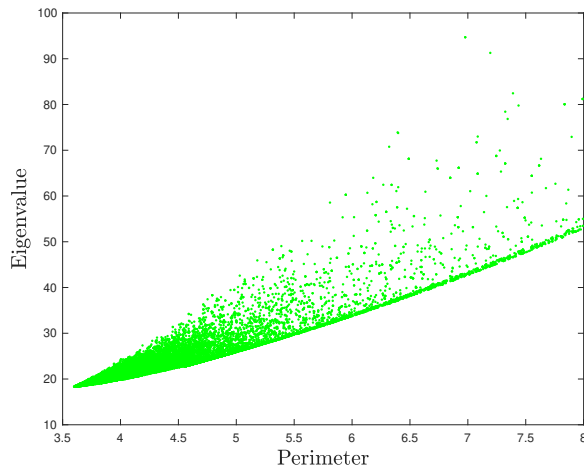


Figure 13: Approximation of the diagram via random convex polygons.

In order to give a more satisfying approximation of the diagram, we want to find the upper and lower domains and thus have a more accurate description of the boundary of the diagram. We are then led to (numerically) solve the following shape optimization problems:

$$\max \setminus \min \{\lambda_1(\Omega) \mid \Omega \in \mathcal{K}, P(\Omega) = p_0 \text{ and } |\Omega| = 1\}, \quad (13)$$

It is shown in [24, Theorem 1.2] that apart from the ball the domains that lay on the lower boundary are polygonal meanwhile the ones that lay on the upper boundary are smooth ( $C^{1,1}$ ), we then apply the method based on the coordinates of the vertices described in Section 3.3 for the lower boundary and the other methods for the upper one and obtain quite satisfying results. In Figure 14, we provide the obtained optimal shapes corresponding to solutions of the problems (13) for some relevant values of  $p_0$ .

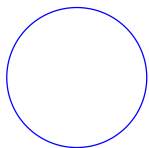
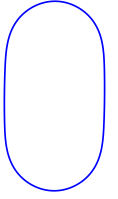
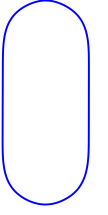
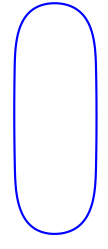
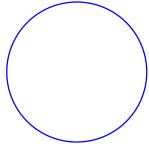
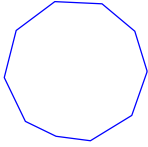
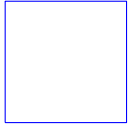
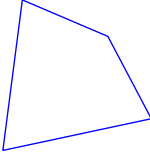
Problem	$p_0 = P(B) = 2\sqrt{\pi}$	$p_0 = 3.8$	$p_0 = 4$	$p_0 = 4.2$
Upper boundary				
Lower boundary				

Figure 14: Numerically obtained optimal shapes corresponding to different values of  $p_0$ .

Finally, once the boundary is known, we use the vertical convexity of the diagram  $\mathcal{D}_2$  (see Theorem 2) to provide an improved and quite optimal numerical description of the diagram, see Figure 15.

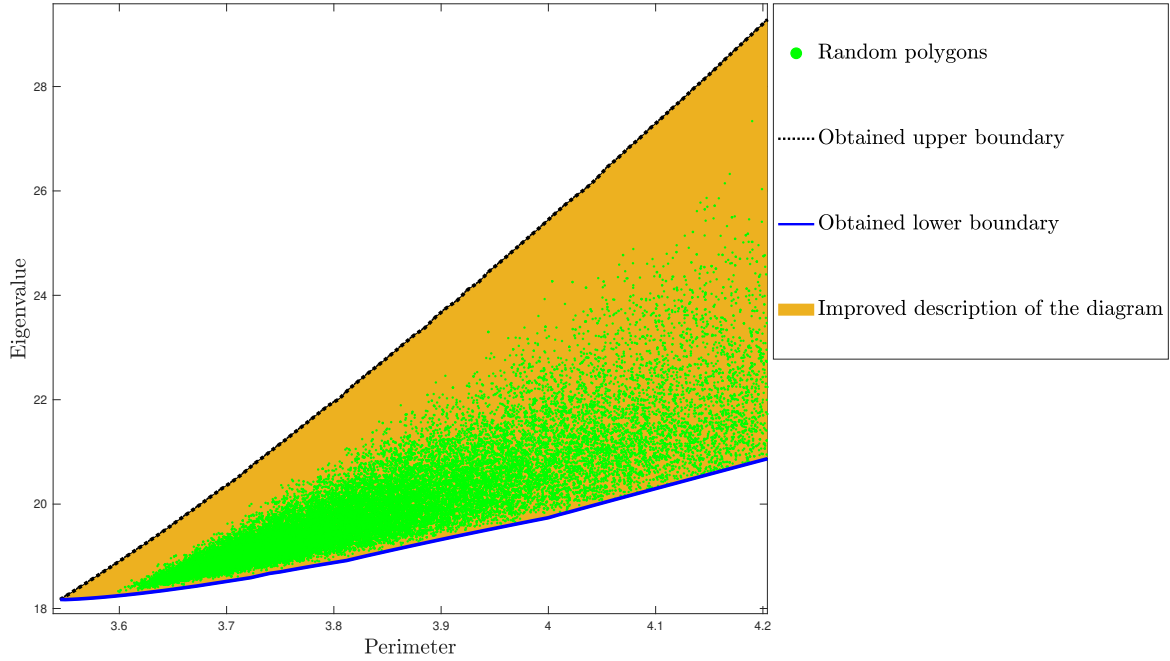


Figure 15: Optimal description of the diagram  $(P, \lambda_1, |\cdot|)$ .

### 4.3 The diagram $\mathcal{D}_3$ of the triplet $(d, \lambda_1, |\cdot|)$

Let us now consider the diagram  $\mathcal{D}_3$  relating the diameter, the first Dirichlet eigenvalue and the area:

$$\mathcal{D}_3 := \{(d(\Omega), \lambda_1(\Omega)) \mid \Omega \in \mathcal{K} \text{ and } |\Omega| = 1\}.$$

As for the previous diagrams, in a first time, we give an approximation of  $\mathcal{D}_3$  by generating  $10^5$  random convex polygons, see Figure 16.

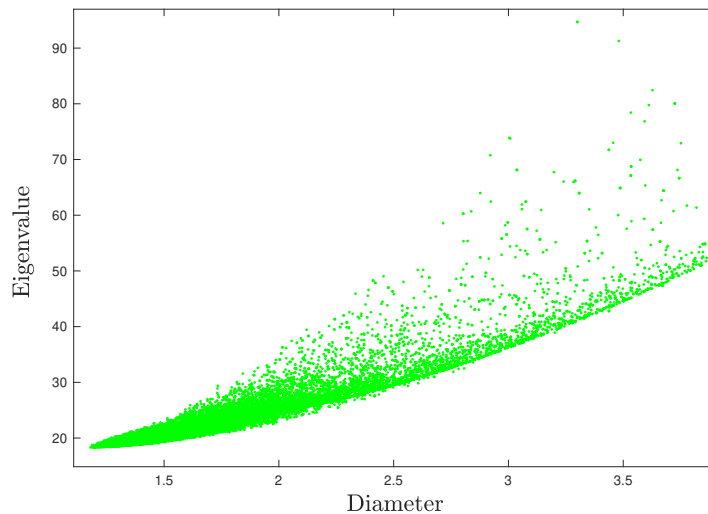


Figure 16: Approximation of the diagram  $\mathcal{D}_3$  via  $10^5$  random convex polygons.

Here also, we are aiming at describing the upper and lower boundaries of the diagram  $\mathcal{D}_3$ , which means to solve the following shape optimization problems:

$$\max \setminus \min \{\lambda_1(\Omega) \mid \Omega \in \mathcal{K}, d(\Omega) = d_0 \text{ and } |\Omega| = 1\}, \quad (14)$$

where  $d_0 \in [2/\sqrt{\pi}, +\infty)$  (because of the isodiametric inequality  $\frac{d(\Omega)}{\sqrt{|\Omega|}} \geq \frac{2}{\sqrt{\pi}}$ ).

For **the lower boundary**, both the methods of parametrization via the Fourier coefficients of the support function (see Section 3.1) and via the discretized radial function (see Section 3.4) provide satisfying results and suggest that the optimal sets are symmetrical 2-cap bodies, that are given by the the convex hulls of a ball and two points symmetric with respect its center (see Figure 17).

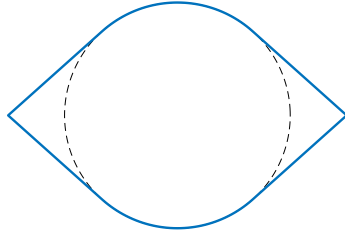


Figure 17: Obtained symmetrical 2-cap body.

On the other hand, **the upper domains** are quite surprising, since we (numerically) observe the existence of a threshold  $d^*$ , such that the solutions for  $d > d^*$  seem to be given by symmetric spherical slices, that are domains defined as the intersection of a disk with a strip of width smaller than the disk's radius and centered at its center, see Figure 18, meanwhile, when  $d < d^*$ , the optimal domains seem to be given by some kind of smoothed regular nonagons, see Figure 18.

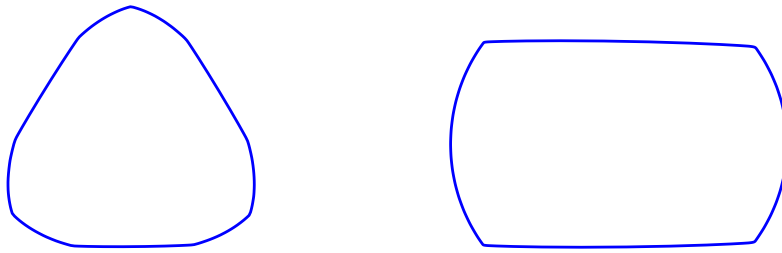


Figure 18: Obtained upper shapes corresponding to  $d_0 = 1.18$  for the smoothed nonagon and to  $d_0 = 1.33$  for the symmetric slice, we used the parametrization via the Fourier coefficients of the support function with 161 coefficient ( $N = 80$ ).

At a first sight, it may be surprising that the optimal shapes do not "continuously" vary in terms of the involved parameters, but, we should note that this phenomena has recently been observed in [21], where the authors provide the complete description of the diagram involving the diameter  $d$ , the inradius  $r$  and the area  $|\cdot|$ ; they prove that one of the boundaries is filled by smoothed nonagons and symmetrical slices meanwhile the other one is filled by symmetrical 2-cap bodies. This leads us to investigate these families of shapes that also seem to be extremal shapes for the diagram  $\mathcal{D}_3$  (see Figure 19). These similarities may be explained by the fact that the functional  $1/r$  corresponds to the first eigenvalue of the infinity-Laplace operator  $\Delta_\infty$  which may be defined as the limit when  $p \rightarrow +\infty$  of the  $p$ Laplacian operator (see [7] and references therein), meanwhile,  $\lambda_1$  corresponds to the first eigenvalues of the 2 Laplace operators, see [34] for more details.

We then compute the values taken by the involved functionals on the symmetrical slices and the smoothed nonagons and obtain Figure 19.

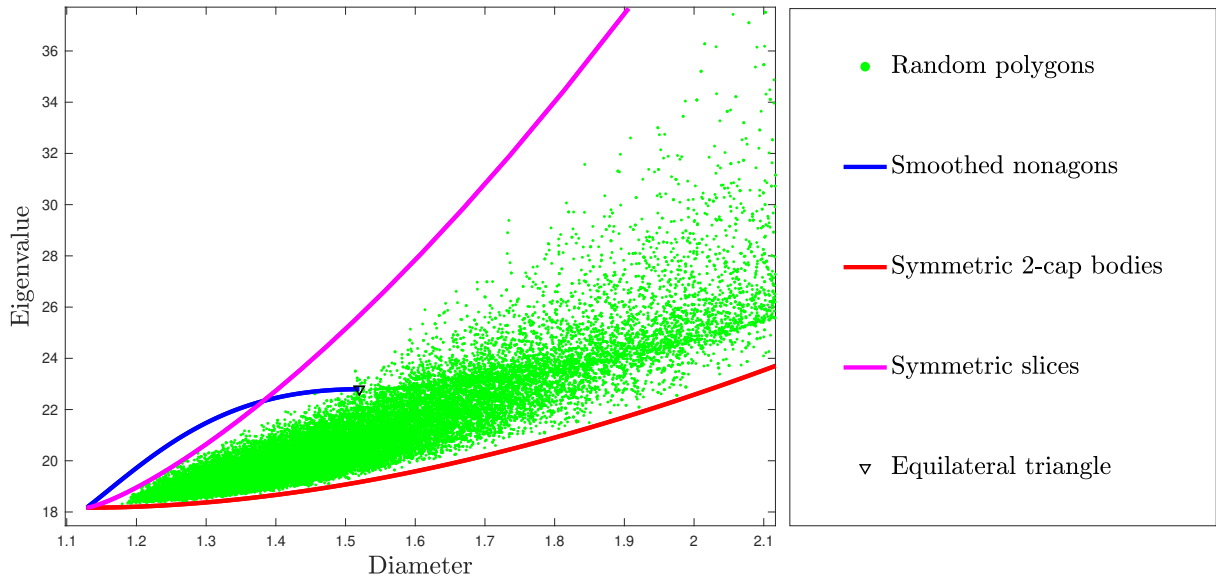


Figure 19: Approximation of the diagram  $\mathcal{D}_3$  with expected extremal sets.

The expected optimal shapes and the best we managed to find are the one given in the following table:

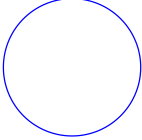
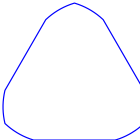
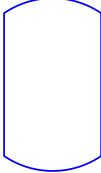

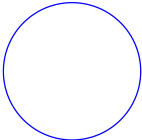
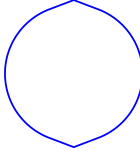
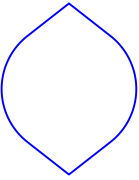
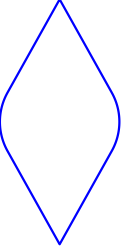
Problem	$d_0 = d(B) = 2/\sqrt{\pi}$	$d_0 = 1.2$	$d_0 = d^* \approx 1.38 \dots$	$d_0 = 1.9$
Upper boundary			 	
Lower boundary				

Figure 20: The best known shapes corresponding to different values of  $d_0$ .

At last, by the vertical convexity of the diagram  $\mathcal{D}_3$  stated in Theorem 2, we are able to provide the following improved approximation of  $\mathcal{D}_3$ .

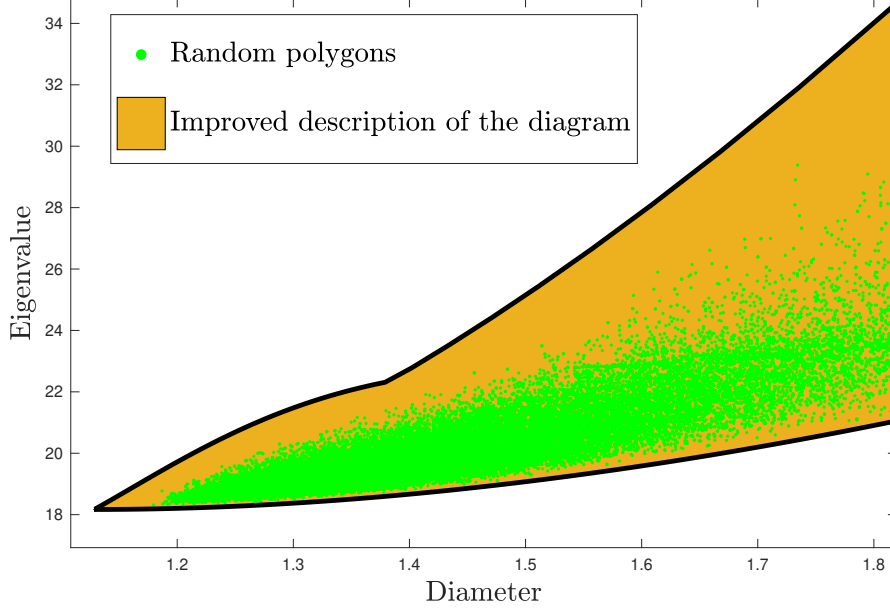


Figure 21: An improved description of the diagram  $\mathcal{D}_3$ .

## Appendix: Computation of the shape derivative of the diameter

In the present appendix, we propose a method to compute the shape derivative of the diameter. This formula is used for numerical shape optimization in the previous sections.

**Theorem 21.** *Let  $V \in C^1(\mathbb{R}^n, \mathbb{R}^n)$  be a smooth vector field. The diameter functional  $d$  admits a directional shape derivative in the direction  $V$  and we have*

$$\begin{aligned} \exists (x_\infty, y_\infty) \in \Omega^2, \quad d'(\Omega, V) &= \lim_{t \rightarrow 0^+} \frac{d(\Omega_t) - d(\Omega)}{t} \\ &= \sup \left\{ \left\langle \frac{x - y}{|x - y|}, V(x) - V(y) \right\rangle \mid x, y \in \Omega, \text{ such that } |x - y| = d(\Omega) \right\} \\ &= \left\langle \frac{x_\infty - y_\infty}{|x_\infty - y_\infty|}, V(x_\infty) - V(y_\infty) \right\rangle, \end{aligned}$$

where  $\Omega_t := (I + tV)(\Omega)$  and  $I : x \in \mathbb{R}^n \mapsto x \in \mathbb{R}^n$  is the identity map.

*Proof.* We want to prove the existence and compute the limit  $\lim_{t \rightarrow 0^+} \frac{d(\Omega_t) - d(\Omega)}{t}$ .

For every  $t \geq 0$   $\Omega_t$  is compact: indeed, it is the image of the compact  $\Omega$  by the continuous map  $I + tV$ . Thus since  $d : (x, y) \in \mathbb{R}^n \times \mathbb{R}^n \rightarrow |x - y|$  is continuous, it is bounded from above and there exists  $(x_t, y_t) \in \Omega$  such that  $d(\Omega_t) = |(I + tV)(x_t) - (I + tV)(y_t)|$ . In what follows, we take  $(x, y) := (x_0, y_0)$ .

We use  $(x_t, y_t)$  (resp.  $(x, y)$ ) as test points to bound  $d(\Omega_t) - d(\Omega)$  from above (resp. below):

$$|(I + tV)(x) - (I + tV)(y)| - |x - y| \leq d(\Omega_t) - d(\Omega) \leq |(I + tV)(x_t) - (I + tV)(y_t)| - |x_t - y_t|.$$

Let us begin by the lower estimate. We have

$$\begin{aligned}
d(\Omega_t) - d(\Omega) &\geq |(I + tV)(x) - (I + tV)(y)| - |x - y| \\
&= |x + tV(x) - y - tV(y)| - |x - y| \\
&= \left| (x - y) + t(V(x) - V(y)) \right| - |x - y| \\
&= \sqrt{\left| (x - y) + t(V(x) - V(y)) \right|^2} - |x - y| \\
&= \sqrt{|x - y|^2 + 2t \langle x - y, V(x) - V(y) \rangle + o(t)} - |x - y| \\
&= |x - y| \sqrt{1 + 2t \left\langle \frac{x - y}{|x - y|}, \frac{V(x) - V(y)}{|x - y|} \right\rangle} + o(t) - |x - y| \\
&= |x - y| \left( 1 + t \left\langle \frac{x - y}{|x - y|}, \frac{V(x) - V(y)}{|x - y|} \right\rangle + o(t) \right) - |x - y| \\
&= t \left\langle \frac{x - y}{|x - y|}, V(x) - V(y) \right\rangle + o(t).
\end{aligned}$$

Thus

$$\liminf_{t \rightarrow 0^+} \frac{d(\Omega_t) - d(\Omega)}{t} \geq \sup \left\{ \left\langle \frac{x - y}{|x - y|}, V(x) - V(y) \right\rangle \mid x, y \in \Omega \text{ such that } |x - y| = d(\Omega) \right\}.$$

Let us now consider the upper estimate. Let  $\left( (x_{t_n}, y_{t_n}) \right)_n$  a subsequence of  $\left( (x_t, y_t) \right)_t$  such that  $t_n \rightarrow 0$  and  $\lim_{n \rightarrow \infty} \frac{d(\Omega_{t_n}) - d(\Omega)}{t_n} = \limsup_{t \rightarrow 0^+} \frac{d(\Omega_t) - d(\Omega)}{t}$ . By Bolzano-Weirstrass Theorem, we assume without loss of generality that there exists  $(x_\infty, y_\infty) \in \Omega^2$  such that the sequence  $\left( (x_{t_n}, y_{t_n}) \right)_n$  converges to  $(x_\infty, y_\infty)$ .

We have  $|x_\infty - y_\infty| = d(\Omega)$ . Indeed:

$$\forall (v, w) \in \Omega^2, \quad |(I + t_n V)(x_{t_n}) - (I + t_n V)(y_{t_n})| \geq |(I + t_n V)(v) - (I + t_n V)(w)|,$$

which is equivalent to

$$\forall (v, w) \in \Omega^2, \quad |x_{t_n} - y_{t_n} + t_n \cdot V(x_{t_n}) - t_n \cdot V(y_{t_n})| \geq |v - w + t_n \cdot V(v) - t_n \cdot V(w)|.$$

Finally

$$\begin{aligned}
d(\Omega_{t_n}) - d(\Omega) &\leq |(I + t_n V)(x_{t_n}) - (I + t_n V)(y_{t_n})| - |x_{t_n} - y_{t_n}| \\
&= |x_{t_n} + t_n \cdot V(x_{t_n}) - y_{t_n} - t_n \cdot V(y_{t_n})| - |x_{t_n} - y_{t_n}| \\
&= \left| (x_{t_n} - y_{t_n}) + t_n \cdot (V(x_{t_n}) - V(y_{t_n})) \right| - |x_{t_n} - y_{t_n}| \\
&= \sqrt{\left| (x_{t_n} - y_{t_n}) + t_n \cdot (V(x_{t_n}) - V(y_{t_n})) \right|^2} - |x_{t_n} - y_{t_n}| \\
&= \sqrt{|x_{t_n} - y_{t_n}|^2 + 2t_n \langle x_{t_n} - y_{t_n}, V(x_{t_n}) - V(y_{t_n}) \rangle + o(t_n)} - |x_{t_n} - y_{t_n}| \\
&= |x_{t_n} - y_{t_n}| \cdot \sqrt{1 + 2t_n \left\langle \frac{x_{t_n} - y_{t_n}}{|x_{t_n} - y_{t_n}|}, \frac{V(x_{t_n}) - V(y_{t_n})}{|x_{t_n} - y_{t_n}|} \right\rangle} + o(t_n) - |x_{t_n} - y_{t_n}| \\
&= |x_{t_n} - y_{t_n}| \cdot \sqrt{1 + 2t_n \left( \left\langle \frac{x_\infty - y_\infty}{|x_\infty - y_\infty|}, \frac{V(x_\infty) - V(y_\infty)}{|x_\infty - y_\infty|} \right\rangle + o(1) \right)} + o(t_n) - |x_{t_n} - y_{t_n}| \\
&= |x_{t_n} - y_{t_n}| \cdot \sqrt{1 + 2t_n \left\langle \frac{x_\infty - y_\infty}{|x_\infty - y_\infty|}, \frac{V(x_\infty) - V(y_\infty)}{|x_\infty - y_\infty|} \right\rangle} + o(t_n) - |x_{t_n} - y_{t_n}| \\
&= |x_{t_n} - y_{t_n}| \cdot \left( 1 + t_n \left\langle \frac{x_\infty - y_\infty}{|x_\infty - y_\infty|}, \frac{V(x_\infty) - V(y_\infty)}{|x_\infty - y_\infty|} \right\rangle + o(t_n) \right) - |x_{t_n} - y_{t_n}| \\
&= t_n \left\langle \frac{x_\infty - y_\infty}{|x_\infty - y_\infty|}, V(x_\infty) - V(y_\infty) \right\rangle + o(t_n).
\end{aligned}$$

Thus

$$\limsup_{t \rightarrow 0^+} \frac{d(\Omega_t) - d(\Omega)}{t} \leq \left\langle \frac{x_\infty - y_\infty}{|x_\infty - y_\infty|}, V(x_\infty) - V(y_\infty) \right\rangle.$$

By combining the lim inf and lim sup inequalities, we obtain:

$$\begin{aligned} \liminf_{t \rightarrow 0^+} \frac{d(\Omega_t) - d(\Omega)}{t} &\geq \sup \left\{ \left\langle \frac{x - y}{|x - y|}, V(x) - V(y) \right\rangle \mid x, y \in \Omega, \text{ such that } |x - y| = d(\Omega) \right\} \\ &\geq \left\langle \frac{x_\infty - y_\infty}{|x_\infty - y_\infty|}, V(x_\infty) - V(y_\infty) \right\rangle \\ &\geq \limsup_{t \rightarrow 0^+} \frac{d(\Omega_t) - d(\Omega)}{t} \\ &\geq \liminf_{t \rightarrow 0^+} \frac{d(\Omega_t) - d(\Omega)}{t}. \end{aligned}$$

Finally, we deduce that the diameter admits a directional shape derivative in the direction  $V$  and

$$\begin{aligned} \exists (x_\infty, y_\infty) \in \Omega^2, \quad \lim_{t \rightarrow 0^+} \frac{d(\Omega_t) - d(\Omega)}{t} &= \sup \left\{ \left\langle \frac{x - y}{|x - y|}, V(x) - V(y) \right\rangle \mid x, y \in \Omega, \text{ such that } |x - y| = d(\Omega) \right\} \\ &= \left\langle \frac{x_\infty - y_\infty}{|x_\infty - y_\infty|}, V(x_\infty) - V(y_\infty) \right\rangle. \end{aligned}$$

□

## Acknowledgments

This work was supported by the Alexander von Humboldt-Professorship program and by the project ANR-18-CE40-0013 SHAPO financed by the French Agence Nationale de la Recherche (ANR). The author is thankful to Jimmy Lamboley and Edouard Oudet for stimulating discussions and comments on the topic of the paper.

## References

- [1] P. Antunes and P. Freitas. New bounds for the principal Dirichlet eigenvalue of planar regions. *Experimental Mathematics*, 15(3):333–342, March 2006.
- [2] P. Antunes and A. Henrot. On the range of the first two Dirichlet and Neumann eigenvalues of the laplacian. *Proceedings of the Royal Society of London*, 467(2):1577–1603, 2011.
- [3] P. R. S. Antunes. Maximal and minimal norm of Laplacian eigenfunctions in a given subdomain. *Inverse Problems*, 32(11):115003, 18, 2016.
- [4] P. R. S. Antunes and B. Bogosel. Parametric shape optimization using the support function. *Comput. Optim. Appl.*, 82(1):107–138, 2022.
- [5] S. Bartels and G. Wachsmuth. Numerical approximation of optimal convex shapes. *SIAM J. Sci. Comput.*, 42(2):A1226–A1244, 2020.
- [6] T. Bayen and D. Henrion. Semidefinite programming for optimizing convex bodies under width constraints. *Optim. Methods Softw.*, 27(6):1073–1099, 2012.
- [7] M. Belloni and E. Oudet. The minimal gap between  $\Lambda_2(\Omega)$  and  $\Lambda_\infty(\Omega)$  in a class of convex domains. *J. Convex Anal.*, 15(3):507–521, 2008.
- [8] C. Bianchini and A. Henrot. Optimal sets for a class of minimization problems with convex constraints. *J. Convex Anal.*, 19(3):725–758, 2012.
- [9] W. Blaschke. Konvexe Bereiche gegebener konstanter Breite und kleinsten Inhalts. *Math. Ann.*, 76(4):504–513, 1915.
- [10] B. Bogosel. Numerical shape optimization among convex sets. working paper or preprint, March 2022.



- [11] K. Böröczky, Jr., M. A. Hernández Cifre, and G. Salinas. Optimizing area and perimeter of convex sets for fixed circumradius and inradius. *Monatsh. Math.*, 138(2):95–110, 2003.
- [12] R. Brandenburg and B. González Merino. A complete 3-dimensional Blaschke-Santaló diagram. *Math. Inequal. Appl.*, 20(2):301–348, 2017.
- [13] R. Brandenburg and B. González Merino. On  $(r, d, R)$ -Blaschke-santaló diagrams with regular  $k$ -gon gauges, 2021.
- [14] L. Brasco, C. Nitsch, and A. Pratelli. On the boundary of the attainable set of the Dirichlet spectrum. *Z. Angew. Math. Phys.*, 64(3):591–597, 2013.
- [15] F. Brock. Continuous Steiner-symmetrization. *Math. Nachr.*, 172:25–48, 1995.
- [16] D. Bucur, G. Buttazzo, and I. Figueiredo. On the attainable eigenvalues of the Laplace operator. *SIAM J. Math. Ana.*, 30:527–536, 1999.
- [17] G. Buttazzo and A. Pratelli. An application of the continuous Steiner symmetrization to Blaschke-Santaló diagrams. *ESAIM, Control Optim. Calc. Var.*, 27:13, 2021. Id/No 36.
- [18] T. Chatelain and A. Henrot. Some results about Schiffer’s conjectures. *Inverse Problems*, 15:647–658, March 1999.
- [19] G. Croce, Z. Fattah, and G. Pisante. A reverse isoperimetric inequality for planar  $(\alpha, \beta)$ -convex bodies. working paper or preprint, March 2022.
- [20] A. Delyon, A. Henrot, and Y. Privat. Non-dispersal and density properties of infinite packings. *SIAM Journal on Control and Optimization*, 57(2):1467–1492, 2019.
- [21] A. Delyon, A. Henrot, and Y. Privat. The missing  $(A, d, r)$  diagram. *Accepted for publication in Ann. Inst. Fourier*, 2020.
- [22] I. Ftouhi. Complete systems of inequalities relating the perimeter, the area and the Cheeger constant of planar domains. working paper or preprint, 2020.
- [23] I. Ftouhi. On the Cheeger inequality for convex sets. *J. Math. Anal. Appl.*, 504(2):Paper No. 125443, 26, 2021.
- [24] I. Ftouhi and J. Lamboley. Blaschke–Santaló diagram for volume, perimeter and first Dirichlet eigenvalue. *SIAM Journal on Mathematical Analysis*, 2020.
- [25] E. M. Harrell, A. Henrot, and J. Lamboley. On the local minimizers of the Mahler volume. *J. Convex Anal.*, 22(3):809–825, 2015.
- [26] E. M. Harrell, II. A direct proof of a theorem of Blaschke and Lebesgue. *J. Geom. Anal.*, 12(1):81–88, 2002.
- [27] A. Henrot. *Extremum problems for eigenvalues of elliptic operators*. Frontiers in Mathematics. Birkhäuser Verlag, Basel, 2006.
- [28] A. Henrot and E. Oudet. Minimizing the second eigenvalue of the Laplace operator with Dirichlet boundary conditions. *Arch. Ration. Mech. Anal.*, 169(1):73–87, 2003.
- [29] M. A. Hernández Cifre. Is there a planar convex set with given width, diameter, and inradius? *Amer. Math. Monthly*, 107(10):893–900, 2000.
- [30] M. A. Hernández Cifre. Optimizing the perimeter and the area of convex sets with fixed diameter and circumradius. *Arch. Math. (Basel)*, 79(2):147–157, 2002.
- [31] M. A. Hernández Cifre and G. Salinas. Some optimization problems for planar convex figures. Number 70, part I, pages 395–405. 2002. IV International Conference in “Stochastic Geometry, Convex Bodies, Empirical Measures & Applications to Engineering Science”, Vol. I (Tropea, 2001).
- [32] M. A. Hernández Cifre and S. Segura Gomis. The missing boundaries of the Santaló diagrams for the cases  $(d, \omega, R)$  and  $(\omega, R, r)$ . *Discrete Comput. Geom.*, 23(3):381–388, 2000.
- [33] M. A. Hernández Cifre, G. Salinas, and S.S Gomis. Complete systems of inequalities. *Journal of inequalities in pure and applied mathematics*, 2(1), March 2001.

- [34] B. Kawohl and V. Fridman. Isoperimetric estimates for the first eigenvalue of the  $p$ -Laplace operator and the Cheeger constant. *Comment. Math. Univ. Carolin.*, 44(4):659–667, 2003.
- [35] T. Kubota. Eine Ungleichheit für die Eiliniien. *Math. Z.*, 20(1):264–266, 1924.
- [36] J. Lamboley and A. Novruzi. Polygons as optimal shapes with convexity constraint. *SIAM Control and Optimization*, 48(5):3003–3025, 2009.
- [37] J. Lamboley, A. Novruzi, and M. Pierre. Regularity and singularities of optimal convex shapes in the plane. *Arch. Ration. Mech. Anal.*, 205(1):311–343, 2012.
- [38] J. Lamboley, A. Novruzi, and M. Pierre. Polygons as maximizers of dirichlet energy or first eigenvalue of dirichlet-laplacian among convex planar domains. (*submitted*), 2022.
- [39] I. Lucardesi and D. Zucco. On Blaschke-Santaló diagrams for the torsional rigidity and the first Dirichlet eigenvalue. *Ann. Mat. Pura Appl. (4)*, 201(1):175–201, 2022.
- [40] E. Makai. On the principal frequency of a membrane and the torsional rigidity of a beam. In *Studies in mathematical analysis and related topics*, pages 227–231. Stanford Univ. Press, Stanford, Calif., 1962.
- [41] S. Pan, X. Sun, and Y. Wang. A variant of the isoperimetric problem. I. *Sci. China Ser. A*, 51(6):1119–1126, 2008.
- [42] G. Pólya. Two more inequalities between physical and geometrical quantities. *J. Indian Math. Soc. (N.S.)*, 24:413–419 (1961), 1960.
- [43] F. P. Preparata and M. I. Shamos. *Computational geometry*. Texts and Monographs in Computer Science. Springer-Verlag, New York, 1985. An introduction.
- [44] L. Santaló. Sobre los sistemas completos de desigualdades entre trespuntos de una figura convexa plana. *Math. Notae*, 17:82–104, 1961.
- [45] R. Schneider. *Convex Bodies: The Brunn-Minkowski Theory*. Cambridge University Press, 2nd expanded edition edition, 2013.
- [46] P. R. Scott and P. W. Awyong. Inequalities for convex sets. *JIPAM. J. Inequal. Pure Appl. Math.*, 1(1):Article 6, 6, 2000.
- [47] J. Steiner. Über parallele Flächen. *Monatsber. preuß. Acad. Wiss.*, Vol. 2:114–118, 1882.
- [48] M. van den Berg, G. Buttazzo, and A. Pratelli. On relations between principal eigenvalue and torsional rigidity. *Commun. Contemp. Math.*, 23(8):28, 2021. Id/No 2050093.

(Ilias Ftouhi) FRIEDRICH-ALEXANDER-UNIVERSITÄT ERLANGEN-NÜRNBERG, DEPARTMENT OF MATHEMATICS, CHAIR OF APPLIED ANALYSIS (ALEXANDER VON HUMBOLDT PROFESSORSHIP), CAUERSTR. 11, 91058 ERLANGEN, GERMANY.

*Email address:* `ilias.ftouhi@fau.de`